Catalysis Today 433 (2024) 114695

Contents lists available at ScienceDirect

Catalysis Today

journal homepage: www.elsevier.com/locate/cattod

Micro and mesoporous materials based on zeolite Y for the florol synthesis via the prins cyclization of isoprenol

Pascal Demuth [a], Luis A. Gallego-Villada [a,b,*], Päivi Mäki-Arvela [a], Ramin Majidov [a], Zuzana Vajglová [a], Narendra Kumar [a], Ilari Angervo [c], Mika Lastusaari [d], Kari Eränen [a], Dmitry Yu. Murzin [a,**]

[a] Laboratory of Industrial Chemistry and Reaction Engineering, Johan Gadolin Process Chemistry Centre, Åbo Akademi University, Henriksgatan 2, Turku, Åbo 20500, Finland
[b] Environmental Catalysis Research Group, Chemical Engineering Faculty, Universidad de Antioquia, Medellín, Colombia
[c] Wihuri Physical Laboratory, Department of Physics and Astronomy, FI-20014 University of Turku, Finland
[d] University of Turku, Department of Chemistry, FI-20014, Turku, Finland

ARTICLE INFO

Keywords:
Prins cyclization
Tin
Zeolite Y
Faujasite
Hierarchical zeolite

ABSTRACT

Several parents and Sn-modified microporous and mesoporous catalysts were investigated in Prins cyclization of isoprenol with isovaleraldehyde for the production of the desired cis isomer of pyranol, Florol ® using dimethylcarbonate as a solvent in the temperature range of 30–60 °C. The highest selectivity to pyranols, 70% was obtained over microporous Sn-Y-80 (number denotes SiO_2/Al_2O_3 ratio) at 40 °C, while 64% selectivity to pyranols was obtained at 99% conversion over dealuminated H-Y-80 exhibiting mesoporosity and low Brønsted to Lewis acid ratio of 0.16. For microporous catalysts even higher BA/LA ratio and large amounts of Lewis acid sites were beneficial, as was the case for H-Y-30 modified with $SnCl_2$, because the reaction occurred mainly on the outer surface of the catalyst.

1. Introduction

The Prins cyclization reaction is currently standing out as the main methodology to synthesize oxygenated heterocycles, especially in the fragrance industry [1]. This reaction constitutes a powerful tool to yield tetrahydropyrans, by mixing a homoallylic alcohol and an aldehyde in the presence of an acid material under anhydrous conditions [2]. Therefore, this reaction can be activated by relatively inexpensive acid heterogeneous catalysts, making the research topic interesting and offering a significant challenge to gain more knowledge about efficient green routes in the synthesis of these high-added value products. The focus of this study lies in the synthesis of commercially valuable tetrahydropyranol (2-isobutyl-4-methyl-tetrahydro-2*H*-pyran-4-ol, commercially known as Florol® or Florosa) using bioderived reactants such as isoprenol (3-methyl-3-buten-1-ol, IP) and isovaleraldehyde (IVA), as illustrated in Fig. 1. Isoprenol offers various advantages such as a low dosage and durability being primarily used as a building block for aromatic chemicals and active pharmaceutical ingredients (APIs) [3]. This alcohol has been used widely in the production of prenol and prenal [4–7], which can be transformed into citral, an important precursor for various odor and flavor chemicals [8–10]. On the other hand, isoprenol can be produced in an aqueous phase from formaldehyde reacting with isobutene, and subsequent separation after the reaction by distillation from mixtures containing also formaldehyde, water, and isobutene in the purification processes [11]. In the last years, some alternative bio-synthetic routes for the production of isoprenol have been investigated based on dimethyl sulfoxide-assisted ionic liquid pretreatment of switchgrass [12], upstream glycolysis pathway of *E. coli* native 2-methyl-(D)-erythritol-4-phosphate [13], and isopentenyl diphosphate-bypass pathway using the promiscuous activity of diphosphomevalonate decarboxylase [14].

Florol® is a colorless to pale yellow, oily liquid that can be extracted from flower petals or industrially synthesized through the Prins reaction. This compound has gained significance in industrial applications

* Corresponding author at: Laboratory of Industrial Chemistry and Reaction Engineering, Johan Gadolin Process Chemistry Centre, Åbo Akademi University, Henriksgatan 2, Turku, Åbo 20500, Finland.
** Corresponding author.
E-mail addresses: alfonso.gallego@udea.edu.co (L.A. Gallego-Villada), dmitry.murzin@abo.fi (D.Yu. Murzin).

https://doi.org/10.1016/j.cattod.2024.114695
Received 18 January 2024; Received in revised form 7 March 2024; Accepted 2 April 2024
Available online 3 April 2024

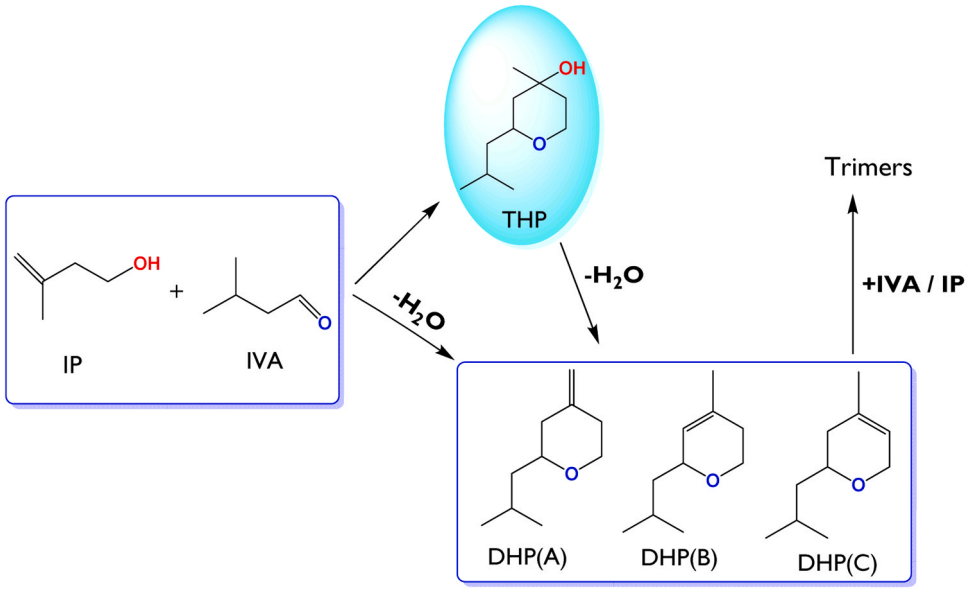

Fig. 1. Scheme for the synthesis of tetrahydropyranol (THP) via Prins cyclization of isoprenol (IP) with isovaleraldehyde (IVA). DHP refers to the dehydration products.

within the fragrance sector [15]. Its global demand is expected to rise in the coming years. The Prins cyclization of isoprenol has been studied using various catalysts, which include homogeneous ones such as sulfuric acid [16] and *p*-toluene sulfonic acid [16], as well as heterogeneous counterparts like ion exchange resins [17], supported heteropolyacids [18,19], Fe-modified silica [20], acid-modified clays (halloysite, montmorillonite, illite) [21], Fe-modified beta zeolite [22], and hierarchical beta zeolites [23]. Isomorphously substituted zeolites [24,25] and metal-organic frameworks [25,26] are interesting catalysts for the Prins condensation reaction involving β-pinene with formaldehyde [26–28], as well as 3-buten-1-ol and anisole with butyraldehyde [24]. The highest yield (71%) of Florol® has been reported over H-Beta-300, which exhibited 82 μmol g^{-1} of acidity measured with pyridine as a probe molecule, a total surface area of 629 m^2 g^{-1}, and a mesopores/micropores volumes ratio of 1.09, under identical reaction conditions [22]. Furthermore, the estimated size of the cis-pyranol is 0.906 nm, while for trans-pyranol it is about 0.939 nm. As the pore size of H-Beta-300 is ca. 0.68 nm, this implies that the reaction is likely taking place on the external surface of the zeolite crystals rather than within the pores. A high yield of Florol® (55.4%) was also achieved over hierarchical beta zeolites (3 h, 40 °C, isovaleraldehyde/isoprenol molar feed ratio = 5) with a catalyst having a Si/Al ratio of 43, moderate acidity (0.29 mmol pyridine g^{-1}), 0.60 cm^3 g^{-1} of mesoporosity, and an external surface area of about 290 m^2 g^{-1} [23].

Metal-modified zeolites have been very scarcely used in Prins cyclization [22,29–31]. In our recent work, Fe-modified H-Beta-300 zeolite afforded slightly lower Florol® selectivity in comparison to the parent H-Beta-300 [22]. It is known that metal modification for zeolites can enhance especially the concentration of Lewis acid sites, which have exhibited a promoting effect in the intermolecular Prins cyclization of citronellal [29] and in the synthesis of nopol from β-pinene and paraformaldehyde [30,31]. In nopol synthesis, Zr-Beta catalyst with an optimum Zn content of ca. 3.7% gives 94% selectivity to nopol at 90 °C under 10 h [31]. This catalyst exhibited a low BA/LA acidity of 0.06. On the other hand, the Sn-Beta catalyst was less efficient for producing nopol at 90 °C giving ca. 77% selectivity to nopol at 63% conversion in 2 h, while mesoporous Sn-MCM-41 was more efficient resulting in 79% selectivity at 94% conversion [30]. This result was interpreted as indicative for diffusional limitations when using Sn-Beta in nopol synthesis. In addition, no information about acidity was given in [30]. For intermolecular citronellal cyclization, very promising results were obtained with aluminum-free Zr-modified Beta zeolite giving 97% yield of isopulegol [29]. This catalyst exhibited more Lewis than Brønsted acid sites; however, no quantitative information about the concentration of acid sites was given in [29].

This study aims to synthesize both cis and trans pyranol through the Prins cyclization process using isoprenol and isovaleraldehyde as starting materials over heterogeneous catalysts, which include tin-modified micro- and mesoporous zeolites Y. Especially the effect of dealumination and extra Lewis acidity achieved by Sn modification has not been systematically investigated previously. The cis isomer of pyranol corresponds to the compound known as Florol®, while the other compounds generated in this reaction are considered side products. Formation of dehydrated products can occur either directly from the reaction between isoprenol and isovaleraldehyde, or indirectly through the dehydration of tetrahydropyranol. Additionally, there is a possibility for isovaleraldehyde and isoprenol to react with the dehydrated products, leading to the formation of trimeric compounds [22].

2. Experimental

2.1. Reagents

Commercial materials were used in the experiments without further processing. The reagents for the synthesis of catalysts were zeolites from Zeolyst International: CBV 400 (SiO_2/Al_2O_3 molar ratio = 5.1, proton form), CBV 720 (SiO_2/Al_2O_3 molar ratio = 30, proton form), CBV 780 (SiO_2/Al_2O_3 molar ratio = 80, proton form); nitric acid solution (HNO_3, 70 wt%, Fischer Scientific); tin (IV) chloride pentahydrate ($SnCl_4{\cdot}5H_2O$, 98 wt%, Sigma-Aldrich); tin (II) chloride ($SnCl_2$, 98 wt%, Sigma-Aldrich); triethylamine (TEA, 99 wt%, Alfa Aesar). Reagents for the catalytic tests were 3-methylbut-3-en-1-ol (isoprenol, $C_5H_{10}O$, 97 wt%, Sigma-Aldrich), isovaleraldehyde ($C_5H_{10}O$, 97 wt%, Sigma-Aldrich), dimethyl carbonate ($C_3H_6O_3$, 99 wt%, Sigma-Aldrich), and nitrogen (N_2, 99.999%, Woikoski). For the quantification through the multipoint calibration curves isoprenol, citronellal (MW = 154 g mol^{-1}) as a model molecule of the dehydrations product, and hydroxycitronellal (MW = 172 g mol^{-1}) as a model molecule of tetrahydropyranol were used. The chosen molecules were selected due to their equal molecular weight, the same number of carbon and oxygen atoms, and similar polarity.

Table 1
Description of the heterogeneous catalysts.

Entry	Code	Catalyst
1	$Y_{5.1}$	H-Y-5.1
2	Y_{30}	H-Y-30
3	Y_{80}	H-Y-80
4	$Y_{5.1}D$	H-Y-5.1-DA
5	$Y_{30}D$	H-Y-30-DA
6	$Y_{80}D$	H-Y-80-DA
7	$Sn_4Y_{5.1}D$	$SnCl_4$-H-Y-5.1-DA
8	$Sn_4Y_{30}D$	$SnCl_4$-H-Y-30-DA
9	$Sn_4Y_{80}D$	$SnCl_4$-H-Y-80-DA
10	$Sn_4Y_{5.1}EIM$	$SnCl_4$-H-Y-5.1-EIM
11	$Sn_2Y_{5.1}EIM$	$SnCl_2$-H-Y-5.1-EIM
12	$Sn_2Y_{30}EIM$	$SnCl_2$-H-Y-30-EIM
13	$Sn_4Y_{30}EIM$	$SnCl_4$-H-Y-30-EIM
14	$Sn_2Y_{80}EIM$	$SnCl_2$-H-Y-80-EIM
15	$Sn_4Y_{80}EIM$	$SnCl_4$-H-Y-80-EIM

DA refers to the dealumination procedure.

2.2. Synthesis of catalysts

2.2.1. Dealuminated zeolite Y-based catalysts

Catalysts based on dealuminated zeolites were synthesized according to the methodology reported by Jimenez-Martin et al. [32], with some modifications (Table 1) [33]. Commercial zeolites (entries 1–3, Table 1) such as H-Y-5.1 ($Y_{5.1}$), H-Y-30 (Y_{30}), and H-Y-80 (Y_{80}) were dealuminated by contacting it with an aqueous HNO_3 solution (10 M, 20 mL g^{-1} of zeolite) for 1 h at room temperature and constant stirring (120–150 rpm). The resulting solid was recovered by filtration, washed with abundant distilled water until neutral pH, and dried at 105 °C overnight. This procedure was repeated two times to ensure the removal of a high amount of the starting aluminum loading. The resulting material was labeled as Y_xD (entries 4–6, Table 1) where x refers to the SiO_2/Al_2O_3 molar ratio (x = 5.1, 30, or 80).

Sn was incorporated by adding the salt precursor to 250 mL of distilled water upon stirring (120–150 rpm) the suspension for 5 h at room temperature. Subsequently, TEA was introduced with stirring (120–150 rpm) for 2 h, with a TEA: $SnCl_45H_2O$ molar ratio of 4. Then, the zeolite was recovered by filtration and dried at 105 °C before calcination in static air using a step calcination procedure, which involves heating the catalyst from room temperature to 200 °C for 100 min and maintaining this temperature for 360 min. Thereafter, the temperature was further raised to 550 °C within 195 min and held for 360 min. Finally, the catalyst was cooled down to 25 °C in 120 min. The resulting solid was labeled as Sn_4Y_xD (entries 7–9, Table 1) where Sn_4 refers to the use of $SnCl_4$ as the Sn salt precursor. More details can be consulted in reference [33].

2.2.2. Zeolite Y-based catalysts

The evaporation impregnation method (EIM) was used for the tin grafting on the commercial support (Y_x, x = 5.1, 30, or 80) using $SnCl_4.5H_2O$ or $SnCl_2$ as precursors [34]. The metal precursor was dissolved in distilled water, after which the zeolite was added to the solution, and the pH was measured. The mixture was then introduced in a rotating evaporator and constantly stirred (50 rpm) at 60 °C for 24 h. After the reaction was completed, the pH was measured, and the water was evaporated from the mixture using a separate vacuum rotary evaporator (50 rpm, 60 °C) until the remaining precipitate was completely dried. The catalyst was calcined using a stepwise calcination procedure, as outlined below: heating from room temperature to 250 °C for 70 min and maintaining this temperature for 60 min. Subsequently, the temperature was further raised to 400 °C over 50 min and held for 180 min. Finally, the catalyst was gradually cooled to 25 °C over 100 min. The resulting solid was labeled as Sn_wY_xEIM (entries 10–15, Table 1). Here, w signifies the Sn salt precursor employed (w = 4 for $SnCl_4.5\ H_2O$ or 2 for $SnCl_2$), and x refers to the SiO_2/Al_2O_3 molar ratio of zeolite Y (x = 5.1, 30, or 80).

2.3. Catalysts characterization

The prepared catalysts were characterized by several characterization techniques. The textural properties were determined by N_2 physisorption with a Micromeritics 3Flex-3500 at −196 °C using ca. 50 mg of the solids. First, the sample was degassed ex-situ in a Micromeritics VacPrep 061 Sample Degas System under vacuum at 180 °C overnight, followed by in-situ degassing in the physisorption equipment under vacuum for 4 h at 250 °C. The specific surface area was calculated using the Dubinin-Radushkevich method and the pore size, pore volume, and pore size distribution were calculated with the non-local density functional theory (N_2-Tarazona NLDFT) method.

The strength and concentrations of both Brønsted and Lewis acid sites were measured using Fourier Transform Infrared Spectroscopy (FTIR) and pyridine as the probe molecule. Pyridine-FTIR spectra were acquired with an ATI Mattson Infinity Series pressing the solid catalysts into thin wafers and placed into the FTIR cell, which was outgassed and heated to 450 °C for 1 h. After that, the cell was cooled to 100 °C and the background spectrum was recorded. Pyridine (>99 wt%, Acros Organics) was adsorbed on the solid surface for 30 min followed by measurements after desorption at 250 °C, 350 °C, and 450 °C under vacuum for 1 h at each temperature. Brønsted acid sites (BA) and Lewis acid sites (LA) were identified using the spectral bands at 1545 cm^{-1} and 1450 cm^{-1}, respectively, and the corresponding concentrations were calculated using the extinction coefficients reported by Emeis [35].

The determination of the average metal particle size was performed by measuring the diameter of over 200 particles using the ImageJ software, from the TEM images (JEM-1400Plus, JEOL instrument) reported

Table 2
Textural properties of the catalytic materials.

Catalyst	SA ($m^2\ g^{-1}$)	d_{av} (nm)	V_{mic} ($cm^3\ g^{-1}$)	V_{mes} ($cm^3\ g^{-1}$)	V_T ($cm^3\ g^{-1}$)	V_{mic}/V_{mes}	Mesoporosity[a] (%)
$Y_{5.1}$ [47]	897	n.a	0.32	0.06	0.38	5.33	15.8
Y_{30}	1115	0.67	0.40	0.10	0.50	4.00	20.0
Y_{80}	678	0.85	0.21	0.09	0.30	2.33	30.0
$Y_{30}D$	874	0.77	0.32	0.11	0.43	2.91	25.6
$Y_{80}D$	591	0.85	0.24	0.11	0.35	2.18	31.4
$Sn_4Y_{30}D$	587	0.85	0.21	0.06	0.27	3.50	22.2
$Sn_4Y_{80}D$	599	0.84	0.22	0.08	0.30	2.75	26.7
$Sn_4Y_{5.1}EIM$	511	0.63	0.21	0.02	0.23	10.50	8.79
$Sn_2Y_{5.1}EIM$	539	0.85	0.19	0.07	0.26	2.71	26.9
$Sn_2Y_{30}EIM$	270	0.84	0.10	0.04	0.14	2.50	28.6
$Sn_4Y_{30}EIM$	615	0.84	0.22	0.08	0.30	2.75	26.7
$Sn_2Y_{80}EIM$	479	0.84	0.17	0.07	0.24	2.43	29.2
$Sn_4Y_{80}EIM$	539	0.84	0.19	0.08	0.27	2.38	29.6

Data taken from [33]. **SA:** Surface area, **d_{av}:** Average pore size, **V_{mic}:** Micropores volume, **V_{mes}:** Mesopores volume, **V_T:** Total pore volume, **n.a:** not available. [a] Calculated as V_{mes}/V_T*100

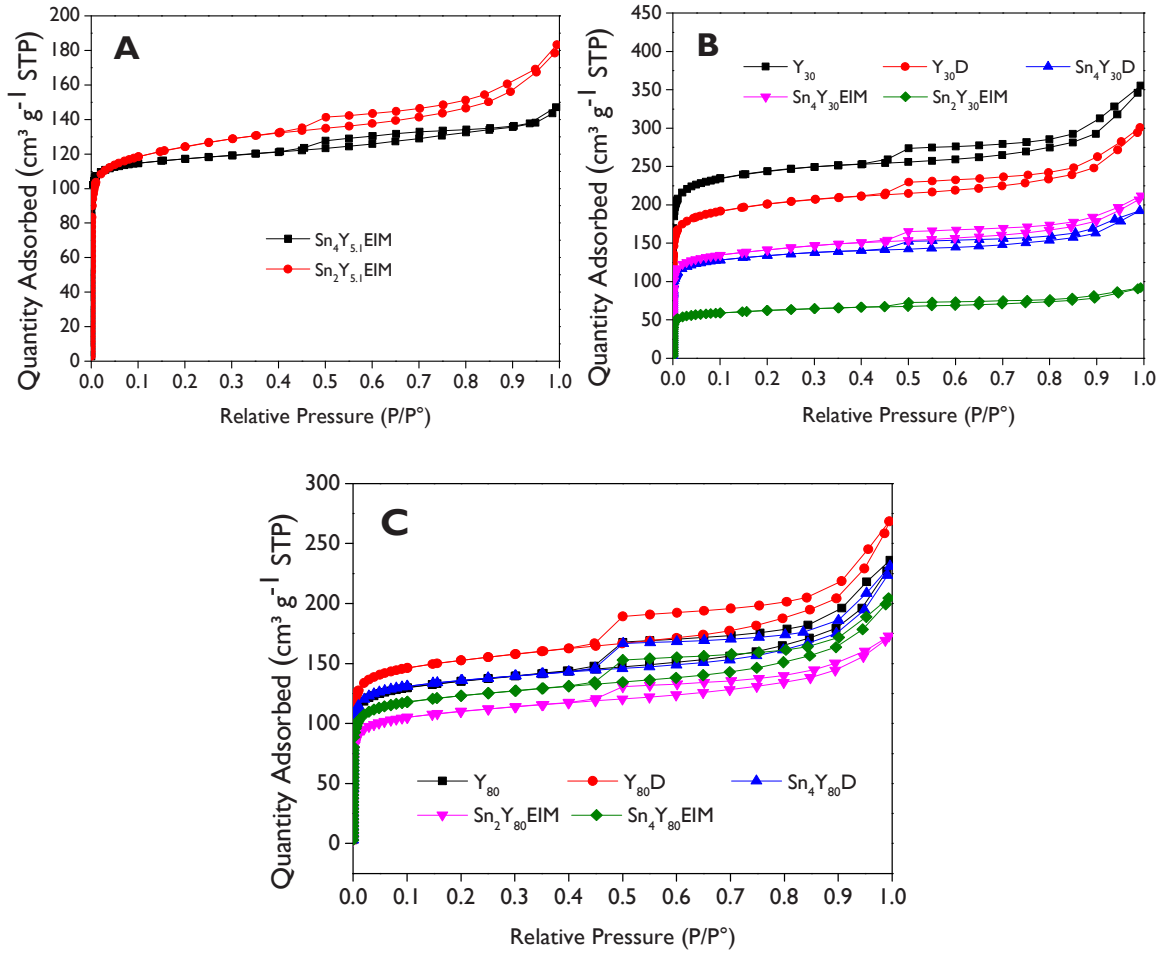

Fig. 2. N_2 adsorption-desorption isotherms for materials based on (A) H-Y-5.1, (B) H-Y-30, (C) H-Y-80. Data taken from [33].

Table 3
Acidity measurements with pyridine-FTIR for the catalytic materials.

Catalyst	Brønsted acidity (μmol g^{-1})				Lewis acidity (μmol g^{-1})				Total (μmol g^{-1})	BA/LA ratio
	Weak	Medium	Strong	Total	Weak	Medium	Strong	Total		
$Y_{5.1}$ [47]	47	85	21	153	8	3	7	18	171	8.5
Y_{30}	25	109	13	147	4	7	1	12	159	12.3
Y_{80}	3	15	6	24	6	9	0	15	39	1.6
$Y_{30}D$	1	5	6	12	0	0	2	2	14	6.0
$Y_{80}D$	1	2	0	3	12	6	1	19	22	0.16
$Sn_4Y_{30}D$	25	14	8	47	22	12	4	38	85	1.2
$Sn_4Y_{80}D$	8	0	0	8	9	0	0	9	17	0.9
$Sn_4Y_{5.1}EIM$	11	55	62	128	3	1	0	4	132	32.0
$Sn_2Y_{5.1}EIM$	47	30	63	140	9	9	13	31	171	4.5
$Sn_2Y_{30}EIM$	4	8	76	88	1	4	15	20	108	4.4
$Sn_4Y_{30}EIM$	11	38	49	98	14	23	2	39	137	2.5
$Sn_2Y_{80}EIM$	51	15	4	70	44	2	0	46	116	1.5
$Sn_4Y_{80}EIM$	7	27	49	83	9	21	2	32	115	2.6

Data taken from [33].

in [33]. Furthermore, the elemental composition was determined by SEM-EDX (Zeiss Leo Gemini 1530 instrument equipped with a Thermo Scientific UltraDry Silicon Drift Detector) as was reported previously for these catalysts [33]. XRD (PANalytical Empyrean diffractometer) and UV-Vis measurements (Avantes Avaspec HS-TEC CCD spectrometer) were performed as described in [33].

The spent catalyst was characterized using temperature-programmed oxidation (O_2-TPO) coupled with mass spectrometry (MS) to detect the coke formation. O_2-TPO was carried out on a BELCAT II analyzer (Microtrac MRB) coupled with a mass spectrometer (Pfeiffer OmniStar GSD 350). First, ca. 120 mg of the sample was pre-treated at 120 °C for 2 h (10 °C min^{-1}), followed by cooling to 35 °C. The analysis was carried out by heating up to 900 °C (5 °C min^{-1}) using a mixture of 5 vol% O_2/Ar (30 mL min^{-1}). The holding time of the target temperature was 10 min.

2.4. Catalytic tests

The Prins cyclization reaction of isoprenol with isovaleraldehyde was carried out in the liquid phase using a glass flask as a batch reactor.

Table 4
Elemental composition of the catalytic materials according to SEM-EDS analysis.

Catalyst	Weight %							SiO_2/Al_2O_3 molar ratio
	Al_2O_3	SiO_2	SnO_2	Si	Al	O	Sn	
$Y_{30}D$	2.23	97.8	0.0	45.7	1.2	53.1	0.00	74.4
$Y_{80}D$	1.9	98.1	0.0	45.96	1.00	53.1	0.00	88.6
$Sn_4Y_{5.1}D$	2.1	95.8	2.1	44.8	1.13	52.5	1.66	75.9
$Sn_4Y_{30}D$	3.0	95.3	1.7	44.6	1.57	52.	1.35	54.5
$Sn_4Y_{80}D$	2.1	95.6	2.3	44.7	1.10	52.4	1.79	78.0
$Sn_2Y_{5.1}EIM$	4.2	73.4	22.4	34.33	2.22	45.8	17.6	29.7
$Sn_2Y_{30}EIM$	3.6	76.0	20.4	35.54	1.90	46.5	16.1	36.0
$Sn_4Y_{30}EIM$	4.1	82.0	13.9	38.31	2.19	48.5	11.0	33.7
$Sn_2Y_{80}EIM$	3.2	76.9	19.9	35.96	1.67	46.7	15.7	41.3
$Sn_4Y_{80}EIM$[a]	2.5	85.2	10.4	39.84	1.31	48.8	8.12	58.6

Data taken from [33]. [a]The balance (1.93) corresponds to Cl.

The flask was equipped with a thermocouple, a sampling valve, an N_2 feeding, and a condenser. The setup was mechanically stirred (1400 rpm) to prevent external mass transfer imitations. In a typical experiment, 0.43 g (5 mmol) of isoprenol and 2.14 g (25 mmol) of isovaleraldehyde were added with dimethyl carbonate as a solvent to reach 25 mL as the total volume of reaction. The solvent and reactants were then pre-heated to 40 ºC under an inert N_2 atmosphere. Once stabilized, 75 mg of the catalyst was rapidly introduced to the reactor after being dried overnight and put in the exicator for 10 min, at least, before its use. Samples of approximately 0.3 mL were collected at various time intervals using a syringe equipped with 0.45 µm filters to analyze time dependent concentration profiles. These samples were then diluted with additional dimethyl carbonate before being analyzed using an Agilent Technologies 6890 N gas chromatograph equipped with a HP-5 column (30 m length x 0.32 mm internal diameter x 0.5 µm film thickness), an FID detector, and an autosampler. The oven-temperature program started at 60 ºC and held for 5 min, then it was heated to 130 ºC at 3 ºC min^{-1}, followed by reaching 280 ºC at 12 ºC min^{-1} and holding for 10 min.

After 180 min, the reaction was stopped and the best performing catalyst ($Y_{80}D$) was recovered by filtration to evaluate its reusability in the catalytic test at 40 ºC, and calcined in static air at 400 ºC using the following step calcination program: heating from room temperature until 250 ºC for 75 min and held for 50 min, followed heating up to 400 ºC for 65 min and holding for 120 min. Finally, the catalyst was cooled down to 25 ºC over 100 min.

The initial rate and the initial TOF for isoprenol were calculated based on Eqs. (1)-(2):

$$r_{0,IP} = \frac{n_{i,IP} - n_{f,IP}}{\Delta t \times m_{cat}} \quad (1)$$

$$TOF_{0,IP} = \frac{n_{i,IP} - n_{f,IP}}{\Delta t \times total\ acidity} \quad (2)$$

Where $n_{i,IP}$ and $n_{f,Ip}$ correspond to moles of isoprenol at time 1 min and 10 min, respectively, Δt is the initial time interval between 1 min and 10 min, m_{cat} is the catalyst mass, and the total acidity denotes the sum of Brønsted and Lewis acidity of the catalyst. In the current work total acidity was considered as a descriptor of catalytic activity. In general, the acid type and strength as well as location of tin in the framework and extra framework can be of importance and TOF thus can be calculated based on the real active sites. Quantification of the true active sites is however very challenging, going clearly beyond the scope of this work.

The isoprenol conversion (X_I), the selectivity to the product i (S_i), and the yield to the product (Y_i) were calculated based on Eqs. (3)-(5).

$$X_I(\%) = \frac{C_{I,0} - C_{I,t}}{C_{I,0}} * 100 \quad (3)$$

$$S_i(\%) = \frac{C_{i,t}}{\sum C_{products,t}} * 100 \quad (4)$$

$$Y_i(\%) = \frac{C_{i,t}}{C_{L,0}} * 100 = \frac{X_L * S_i}{100} \quad (5)$$

Where $C_{I,0}$, $C_{I,t}$, and $C_{i,t}$ represent the initial molar concentration of isoprenol, the molar concentration of isoprenol after time *t*, and the molar concentration of the product *i* after time *t*, in the reaction mixture, respectively. The concentrations of isoprenol as the substrate and the products such as tetrahydropyranol and dehydration products were determined from the multipoint calibration curves.

3. Results and discussion

3.1. Catalyst characterization

XRD results (Figure S1A) from [33], revealed the presence of both faujasite zeolite [36] and SnO_2 phase [37]. Especially, the diffraction patterns of $Sn_2Y_{30}EIM$ and $Sn_4Y_{30}EIM$ revealed clearly the presence of the SnO_2 phase [37], while identification of SnO_2 was not reliable in $Sn_4Y_{30}D$ due to its low signal intensity. A plot illustrating the lattice parameter (a_0) vs. the SiO_2/Al_2O_3 molar ratio for different catalysts based on zeolite Y is depicted in Figure S1B. An inverse trend between two parameters is observed, with the a_0 parameter increasing as the SiO_2/Al_2O_3 ratio decreases. Our results align with the values reported in the literature [38–40]. The change in the lattice parameter is due to the different bond lengths of tetrahedral Si-O and Al-O bonds being 1.6 Å and 1.7 Å, respectively [41]. On the other hand, UV-Vis of the spent $Sn_2Y_{80}EIM$ and $Sn_4Y_{80}EIM$ catalysts [33] demonstrated that the former one exhibited a high amount of isolated Sn-species related to the band at 205 nm [42], while the intensity of the peak at 205 nm for $Sn_4Y_{80}EIM$ was slightly lower. The shoulder at ca. 320 nm is also visible for the current samples showing the presence of hydrated isolated Sn^{4+} with a high coordination number [42]. No bands were observed for the supports, as expected.

3.1.1. Nitrogen physisorption

The textural properties of the prepared catalysts are presented in Table 2 and Fig. 2. The presence of mesopores in all materials is confirmed by the adsorption-desorption isotherms (Fig. 2), which exhibited a type IV hysteresis, associated with capillary condensation inside the pores [43]. The surface areas (Table 2) were calculated by the Dubinin-Radushkevich method, which is widely recommended for this type of zeolitic materials because it was derived from the micropore filling theory [44]. Furthermore, the BET model assuming infinite number of layers can often fail in many systems due to obvious limitations [45]. The catalyst with the highest surface area was the pristine zeolite with a SiO_2/Al_2O_3 molar ratio of 30 (Y_{30}) exhibiting a value of 1115 $m^2\ g^{-1}$. Once the dealumination process was carried out with nitric acid (10 M), a considerable decrease of ca. 22% in the area was obtained, yielding a value of 874 $m^2\ g^{-1}$, and showing the successful formation of larger pores (mesopores). Similar behavior can be observed

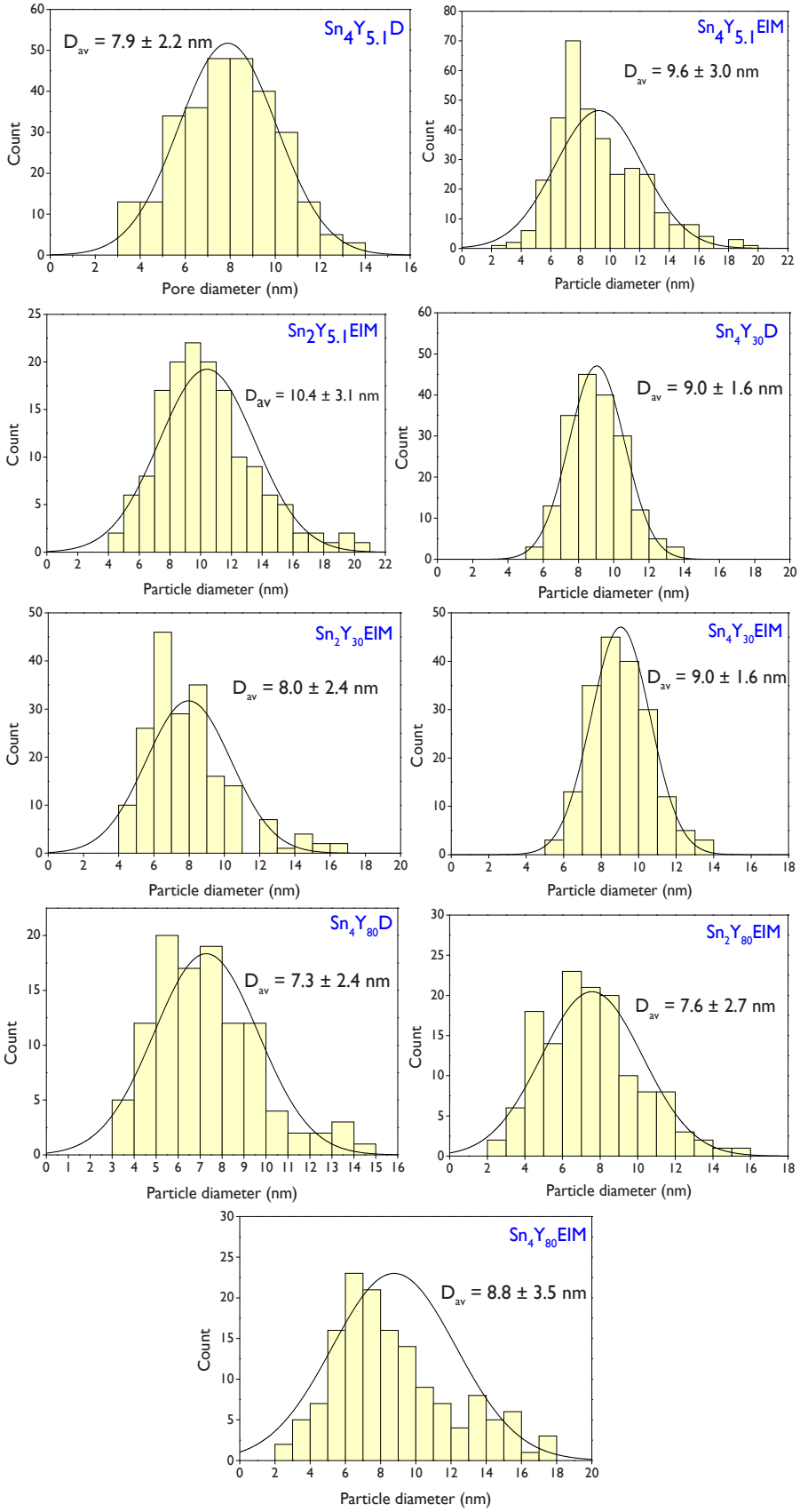

Fig. 3. Histograms for the particle size distribution of tin-modified zeolite Y catalysts. Data taken from [33].

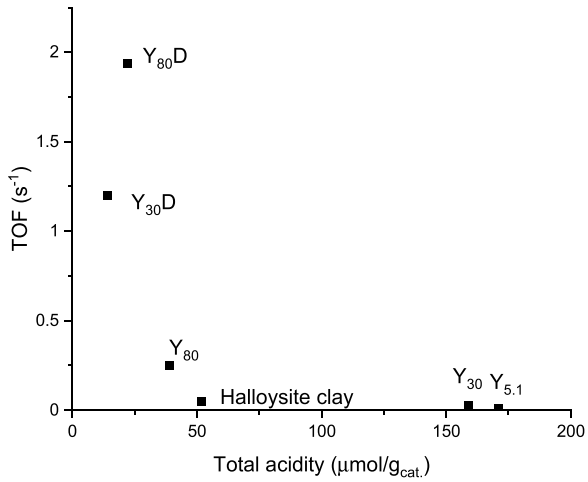

Fig. 4. The initial TOF as a function of total acidity for micro- and mesoporous zeolites at 40 °C. Halloysite clay was studied in trans-4-hydroxymethyl-2-carene reaction with salicylic aldehyde at 25 °C [48].

for the zeolite of molar ratio of 80 with values of 680 and 590 $m^2\ g^{-1}$ for the pristine and dealuminated materials, respectively. Incorporation of tin, either $SnCl_4 5\ H_2O$ or $SnCl_2$, on the different series of parent and dealuminated zeolites, caused significant decreases in the surface area, owing to the pore blocking or clogging.

On the other hand, the average pore sizes are very similar for all the materials, with values averaging around 0.84 nm, except for Y_{30}, Y_{30}D, and $Sn_4Y_{5.1}$EIM. Therefore, the results suggest that the incorporation of Sn using the two salt precursors did not have a significant effect on the average size of the parent and dealuminated supports. Furthermore, a clear tendency can be observed regarding mesoporosity (Table 2), which increases (or the ratio of micro to mesopore volumes decreases) as the SiO_2/Al_2O_3 molar ratios increase. In addition, the specific surface area decreased for Sn_4Y_{30}D by 33% in comparison to Y_{30}D, while the corresponding change in the surface area for Sn_4Y_{80}D was 9% increase in comparison to Y_{80}D. At the same time, the SiO_2/Al_2O_3 ratio for Sn_4Y_{30}D decreased by 28% when compared to the parent material (see Section 3.1.4), while for Sn_4Y_{80}D it decreased only by 12% indicating that dealumination occurred still during tin loading in the presence of triethylamine and it was more efficient for the former material, which contained originally with a higher aluminum content. It is well-known that dealumination breaks the structure decreasing the surface area [46]. On the other hand, the specific surface area of Sn-modified Y_{30}EIM and Y_{80}EIM catalysts decreased with increasing Sn content, as expected (compare Table 2 data with the results of elemental analysis, Section 3.1.4.)

3.1.2. Catalysts acidity

Acidity of the prepared catalysts was measured through adsorption-desorption FTIR using pyridine as a probe molecule, and the results are presented in Table 3. The total acidity in the parent zeolites Y is directly related to the amount of aluminum. As the SiO_2/Al_2O_3 molar ratio increases, the total acidity decreases from 171 μmol g^{-1} ($Y_{5.1}$) to 39 μmol g^{-1} (Y_{80}). All materials exhibited more Brønsted acid (BA) sites than Lewis acid (LA) sites, as indicated by the BA/LA ratio, except for Sn_4Y_{80}D.

On the other hand, when Y_{30} was dealuminated with nitric acid, there was a significant decrease of ca. 91% in total acidity, resulting in the value of 14 μmol g^{-1}. The BA/LA ratio was nearly halved (from 12.3 to 6.0), suggesting that a larger fraction of Al was removed from the framework during the dealumination process. For the tin-modified materials based on $Y_{5.1}$ and Y_{30}, the presence of Sn did not lead to an increase in the total acidity of the materials. In contrast, for Y_{80} materials, the total acidity increased by approximately three times of the corresponding parent solid (115–116 μmol g^{-1} compared to 39 μmol g^{-1}). These results can be attributed to the high loading of Sn in the materials based on Y_{80}, as shown in Table 4, such as Sn_2Y_{80}EIM and Sn_4Y_{80}EIM, with 15.7 and 8.12 wt%, respectively. Additionally, the use of the two Sn precursors showed noticeable differences in the total acidity for $Y_{5.1}$ (132 and 171 μmol g^{-1}) and Y_{30} (137 and 108 μmol g^{-1}) materials, but not for Y_{80} (116 and 115 μmol g^{-1}) analogs. On the other hand, incorporation of Sn onto Y_{30}D resulted in a significant increase in the total acidity (85 μmol g^{-1}), approximately six-fold that of the dealuminated material (14 μmol g^{-1}).

3.1.3. Distribution of tin particle sizes

TEM images of catalytic materials are presented in Figure S2, showing well-dispersed metal particles in the tin-modified catalysts based on zeolite Y with different SiO_2/Al_2O_3 molar ratios. Micrographs of the dealuminated zeolites ($Y_{5.1}$D, Y_{30}D, and Y_{80}D) clearly illustrate the formation of mesopores in their structure due to the large cavities, without observing collapse after dealumination with nitric acid (Figures S3-S5, Supporting Information). TEM images were used to determine the distribution of tin particle sizes, as shown in Fig. 3. All catalysts exhibited an average tin particle size in the range of 7.3–10.4 nm. The Sn particle size was the largest for the most acidic support based on zeolite Y ($Sn_2Y_{5.1}$EIM) with an average value of 10.4 nm, whereas this value decreased as the SiO_2/Al_2O_3 molar ratio

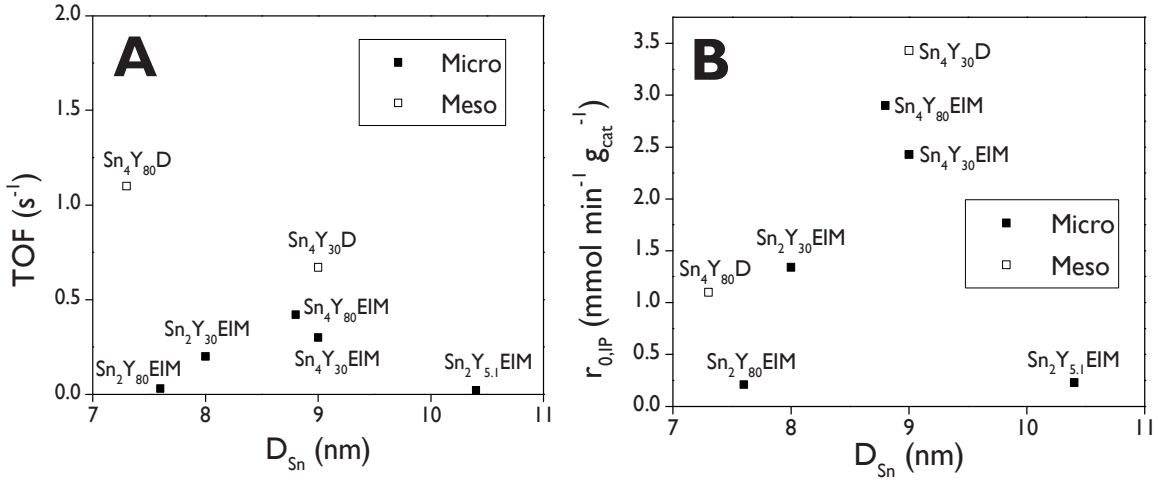

Fig. 5. Initial TOF and $r_{0,IP}$ as a function of average Sn particle size.

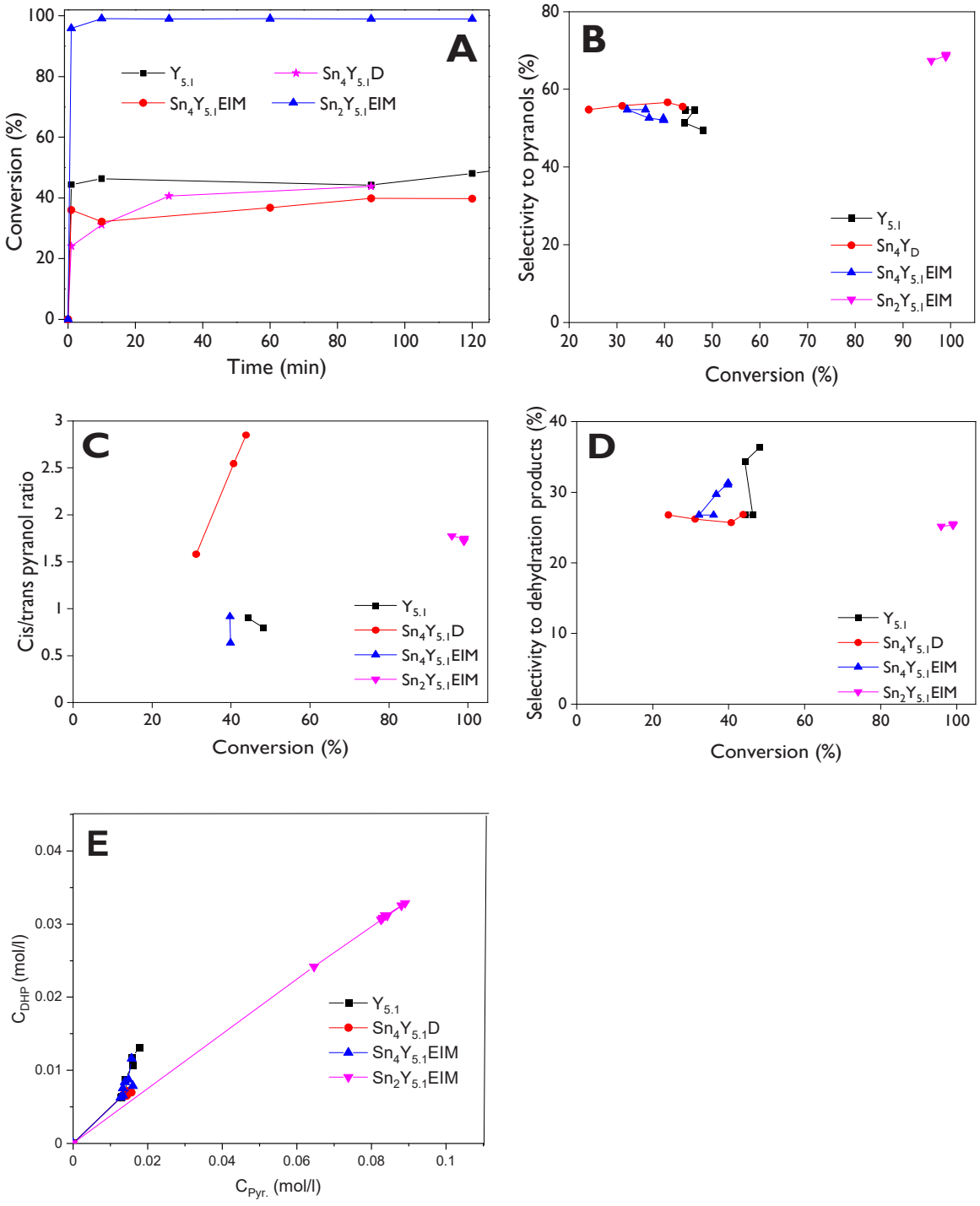

Fig. 6. Dependence of the isoprenol conversion on the reaction time (A), selectivity to pyranols (B), cis/trans pyranol ratio (C), and selectivity to dehydration products (D) as a function of conversion, and concentration of dihydropyrans vs concentration of pyranols (E) over the prepared catalysts based on zeolite H-Y-5.1. Reaction conditions: $C_{Isoprenol,0} = 0.2$ mol L^{-1}, $C_{Isovaleraldehyde,0} = 1.0$ mol L^{-1}, 25 mL total volume, dimethyl carbonate as solvent, 75 mg of catalyst, 40 °C, 1400 rpm.

increased, reaching values of 8.0 and 7.6 nm for $Sn_2Y_{30}EIM$ and $Sn_2Y_{80}EIM$, respectively. Application of Sn (IV) as a tin precursor resulted in an increase in the average size for Y_{30} and Y_{80} materials with a decrease for $Y_{5.1}$ material. In this way, relatively large Sn particle sizes could be explained by its high loading during synthesis. On the other hand, for the tin dealuminated materials using $SnCl_4$ as the salt precursor, an average size between 7.3 and 9.0 nm was reached, without clear trends. Furthermore, some agglomeration can be evidenced in the images for Y_{80} materials, both for $SnCl_4$ and $SnCl_2$ precursors.

3.1.4. *Elemental composition by SEM-EDX*

SEM images of the catalysts, presented in Figure S6, show several shapes, such as triangular, hexagonal, and rectangular, with crystal sizes varying considerably between 190 nm and 800 nm. The materials prepared by EIM with $SnCl_2$ as a precursor ($Sn_2Y_{5.1}EIM$, $Sn_2Y_{30}EIM$, and $Sn_2Y_{80}EIM$) exhibited a visible uniform distribution of tin, which was not possible to observe for the $SnCl_4$ precursor, either in the parent zeolites or the dealuminated ones. On the other hand, the crystal size of the materials prepared with $SnCl_4$ was larger than that of the analogous catalysts prepared with the $SnCl_2$ precursor, which could be linked to

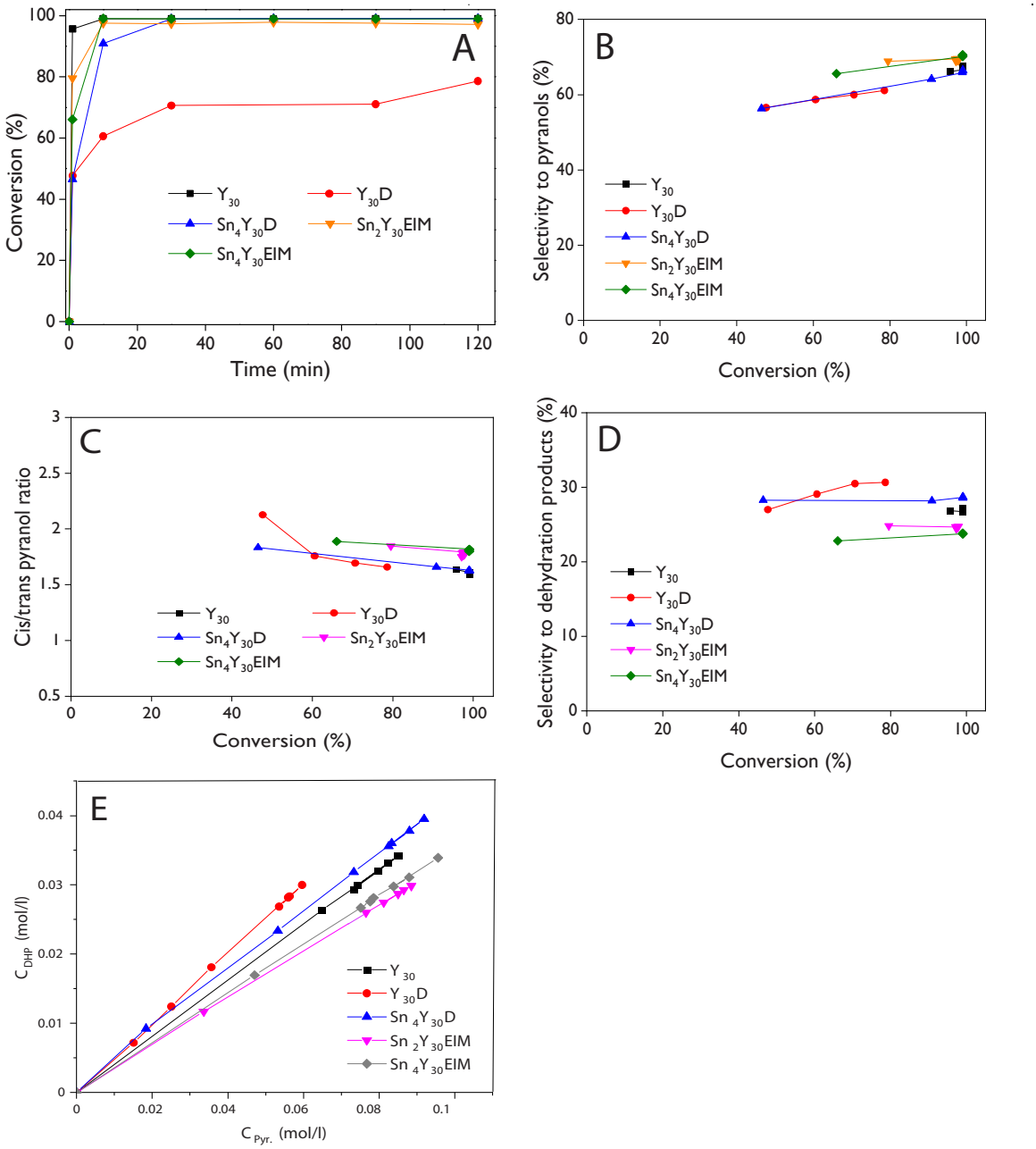

Fig. 7. Dependence of the isoprenol conversion on the reaction time (A), selectivity to pyranols (B), cis/trans pyranol ratio (C), and selectivity to dehydration products (D) as a function of conversion, and concentration of dihydropyrans vs concentration of pyranols (E) over the prepared catalysts based on zeolite H-Y-30. Reaction conditions: $C_{Isoprenol,0} = 0.2$ mol L^{-1}, $C_{Isovaleraldehyde,0} = 1.0$ mol L^{-1}, 25 mL total volume, dimethyl carbonate as solvent, 75 mg of catalyst, 40 °C, 1400 rpm.

higher reactivity of the latter.

SEM images of dealuminated zeolites ($Y_{30}D$ and $Y_{80}D$) illustrate the success of dealumination because the formed mesopores can be observed. This is due to the larger particles breaking down to create more mesoporosity, as was previously analyzed by N_2 physisorption and reported in Table 2. It is worth mentioning that no structural collapse occurred in the materials after treatment with nitric acid.

The elemental composition was determined by SEM-EDX analysis (Table 4), and quantification was reported in terms of wt% of oxides (SiO_2, Al_2O_3, SnO_2) but also atomic wt%.

The materials prepared by EIM showed the highest amount of Sn, varying between ca. 8% and ca. 18%, with the highest amounts prepared with $SnCl_2$. In contrast, the tin-modified dealuminated zeolites displayed low Sn loadings between 1.35% and 1.8%. For $Y_{30}D$ and $Y_{80}D$ materials the SiO_2/Al_2O_3 molar ratios were larger than the initial value for the parent zeolite, 30 and 80, respectively, which is expected as a result of dealumination. This value was noticeably modified when tin was incorporated using either $SnCl_2$ or $SnCl_4$. Furthermore, $Sn_4Y_{80}EIM$ showed impurities of chloride, which could negatively affect its catalytic performance.

3.2. Catalytic performance

3.2.1. Repeatability test, initial TOF and reaction rates

Repeatability of the experimental procedure was confirmed with $Y_{80}D$ catalyst as follows from Figure S7.

The highest initial TOF values for isoprenol transformation were obtained for the catalysts exhibiting mesoporosity and relatively low total acidity as expected (Fig. 4). When comparing these values with those in [48] in Prins cyclization of trans-4-hydroxymethyl-2-carene

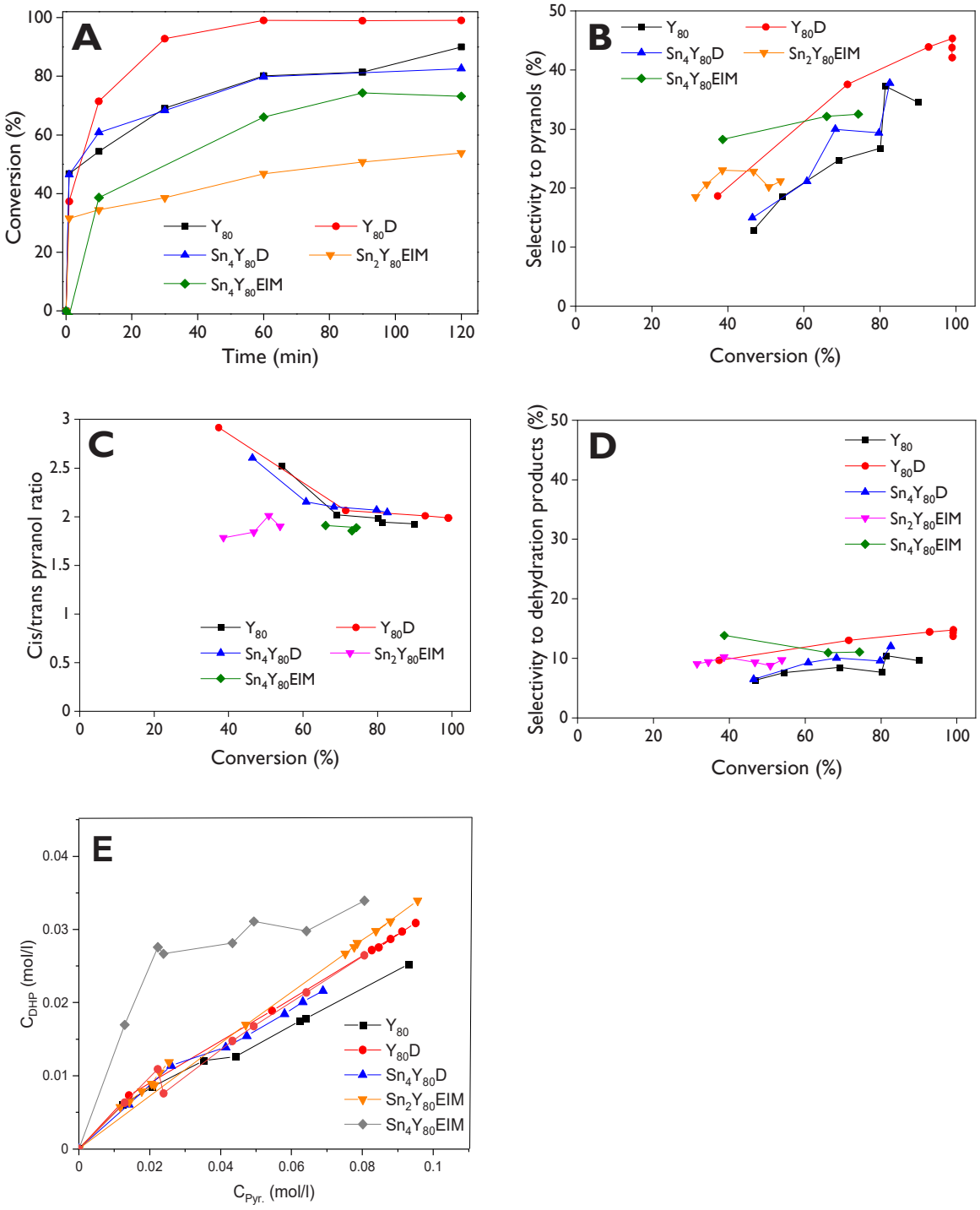

Fig. 8. Dependence of the isoprenol conversion on the reaction time (A), selectivity to pyranols (B), cis/trans pyranol ratio (C), and selectivity to dehydration products (D) as a function of conversion, and concentration of dihydropyrans vs concentration of pyranols (**E**) over the prepared catalysts based on zeolite H-Y-80. Reaction conditions: $C_{Isoprenol,0} = 0.2$ mol L^{-1}, $C_{Isovaleraldehyde,0} = 1.0$ mol L^{-1}, 25 mL total volume, dimethyl carbonate as solvent, 75 mg of catalyst, 40 °C, 1400 rpm.

with salicylic aldehyde at 25 °C over halloysite clay (Fig. 4), the initial TOF in [48] was 0.05 s^{-1} being only 2.4% of the corresponding value obtained for $Y_{80}D$. Noteworthy is that despite mesoporosity and similar total acidity for halloysite as for $Y_{80}D$ and Y_{80}, the initial TOF for this reaction was very low. In addition, microporous mildly acidic H-Beta-300 exhibited no activity for this reaction [48]. It should also be pointed out here that in the case of trans-4-hydroxymethyl-2-carene the ratio between the reactant and the catalyst was 1.8 mmol/g_{cat}, while in the case of isoprenol it was 66 mmol/$g_{cat.}$ One reason for the lower TOF can also be lower reactant purity, 87% reported in [48].

For Sn-modified catalysts the initial TOF was also plotted as a function of average Sn particle size (Fig. 5a). The results showed that a mesoporous tin modified catalyst with the smallest Sn particle size exhibited the highest initial TOF and the opposite effect was observed for the initial rate (Fig. 5b). This catalyst also exhibited a low total acidity. When the Sn particle size increased, the TOF decreased for the mesoporous catalysts. For microporous catalysts, an optimum Sn particle size was observed giving the highest initial TOF and initial rate.

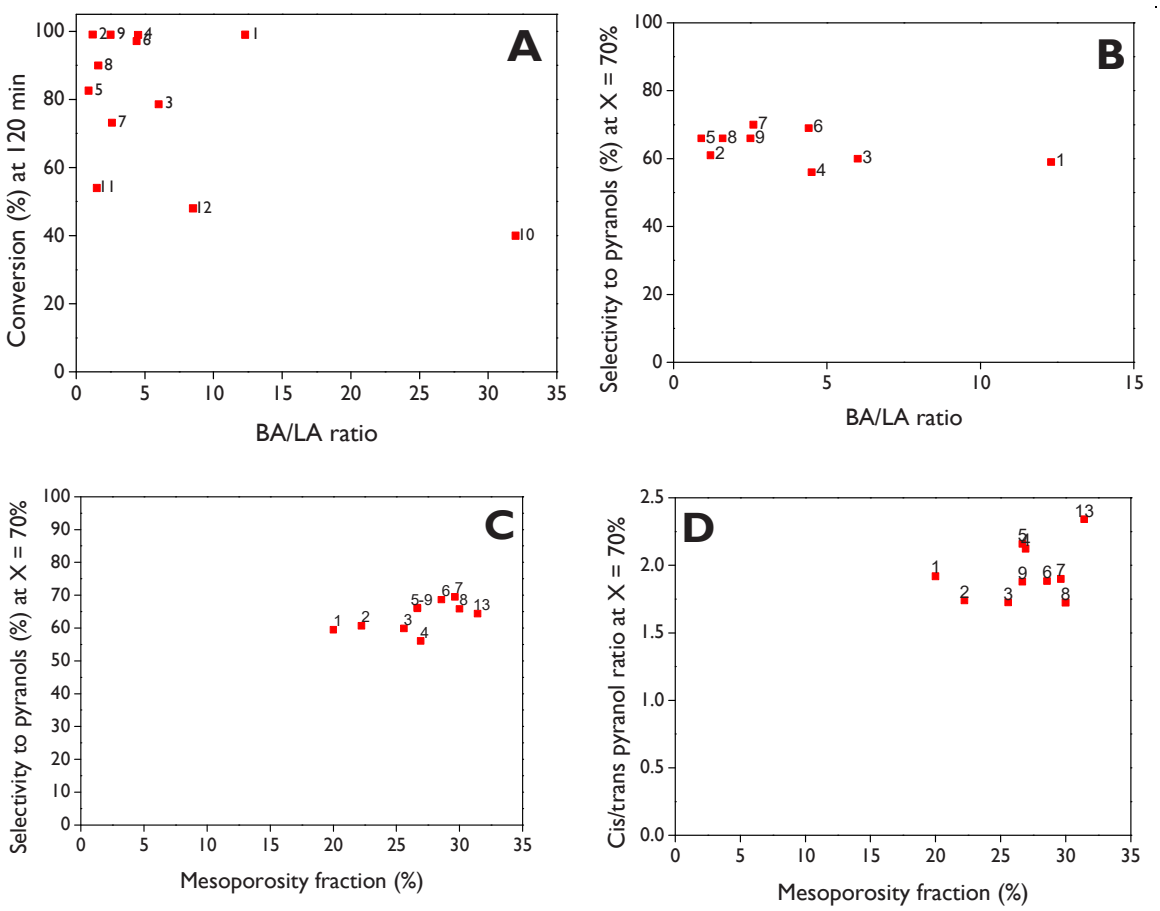

Fig. 9. (A) Conversion of isoprenol at 120 min as a function of the Brønsted-to-Lewis acidity ratio, (B) yield to pyranols at 70% isoprenol conversion as a function of Brønsted-to-Lewis acidity ratio, (C) selectivity to pyranols at 70% isoprenol conversion as a function of the mesoporosity fraction, and (D) cis/trans pyranol ratio at 70% isoprenol conversion as a function of the mesoporosity fraction, for (1) Y_{30}, (2) $Sn_4Y_{30}D$, (3) $Y_{30}D$, (4) $Sn_2Y_{5.1}EIM$, (5) $Sn_4Y_{80}D$, (6) $Sn_2Y_{30}EIM$, (7) $Sn_4Y_{80}EIM$, (8) Y_{80}, (9) $Sn_4Y_{30}EIM$, (10) $Sn_4Y_{5.1}EIM$, (11) $Sn_2Y_{80}EIM$, (12) $Y_{5.1}$, (13) $Y_{80}D$. Reaction conditions: $C_{Isoprenol,0} = 0.2$ mol L^{-1}, $C_{Isovaleraldehyde,0} = 1.0$ mol L^{-1}, 25 mL total volume, dimethyl carbonate as solvent, 75 mg of catalyst, 40 °C, 1400 rpm.

Table 5
Catalyst screening in the Prins cyclization of isoprenol with isovaleraldehyde. **Reaction conditions:** $C_{IP,0} = 0.2$ mol L^{-1}, $C_{IVA,0} = 1.0$ mol L^{-1}, 25 mL total volume, dimethyl carbonate as a solvent, 75 mg of catalyst, 40 °C, 1400 rpm.

Catalyst	$-r_{Isop,0}$ (mmol min^{-1} g^{-1})[a]	TOF_0 (s^{-1})	X (%) at 2 h	$r_{0,DHP}/r_{0,Pyr.}$	S_{Pyr} (%) at X = 70%	S_{DHP} (%) at X = 70%	Cis/trans pyranol ratio at X = 70%	Y_{Pyr} (%) at 2 h	Y_{DHP} (%) at 2 h
$Y_{5.1}$	0.15	0.01	48	0.45	n.a.	n.a.	n.a.	24	17
Y_{30}	0.25	0.03	99	0.38	59	26	1.92	67	27
Y_{80}	0.58	0.25	90	0.29	66	22	1.72	64	18
$Y_{30}D$	0.99	1.16	79	0.52	60	30	1.73	48	24
$Y_{80}D$	2.57	1.94	99	0.29	64	25	2.34	70	23
$Sn_4Y_{30}D$	3.43	0.67	99	0.41	61	28	1.74	66	28
$Sn_4Y_{80}D$	1.08	1.06	83	0.44	66	24	2.16	58	18
$Sn_4Y_{5.1}EIM$	0.12	0.01	40	0.49	n.a.	n.a.	n.a.	n.a.	12
$Sn_2Y_{5.1}EIM$	0.23	0.02	99	0.33	56	23	2.12	68	25
$Sn_2Y_{30}EIM$	1.34	0.21	97	0.35	69	25	1.88	67	24
$Sn_4Y_{30}EIM$	2.34	0.30	99	0.33	66	23	1.88	70	24
$Sn_2Y_{80}EIM$	0.21	0.03	54	0.29	n.a.	n.a.	n.a.	n.a.	14
$Sn_4Y_{80}EIM$	2.43	0.42	73	0.49	70	24	1.90	52	17

[a] acidity not available, **Isop:** Isoprenol, **Pyr:** Pyranols, **DHP:** Dehydration Products, **X:** Isoprenol conversion, $_{Si}$**:** Selectivity to specie i, $\mathbf{Y_i}$**:** Yield to specie i. [a]

3.2.2. *Reaction rates after prolonged times and conversion*

The reaction rates after prolonged reaction times are very different and the final conversion over different catalysts after 120 min varied between 50% and 99% (Figs. 6-9). For the most acidic support $Y_{5.1}$, only $Sn_2Y_{5.1}EIM$ gave a high conversion (> 99%), while other catalysts $Y_{5.1}$, $Sn_4Y_{5.1}D$, and $Sn_4Y_{5.1}EIM$ were less active resulting in the conversion levels in the range of 39–48% (Fig. 6) after 120 min. Rapid catalyst deactivation was observed for these catalysts already after 1 min. When comparing the final conversion with the BA/LA ratio of the catalyst (Fig. 9), high conversion was obtained with an optimum BA/LA ratio. Some exceptions with a low BA/LA ratio and high conversion can be found, i.e. for $Sn_4Y_{80}D$, Y_{80} and $Sn_4Y_{30}D$. In Y_{30} series all other catalyst were very active apart from $Y_{30}D$ (Fig. 7a), which exhibited very low total acidity (Table 3). For H-Y-80 catalysts, the highest conversion

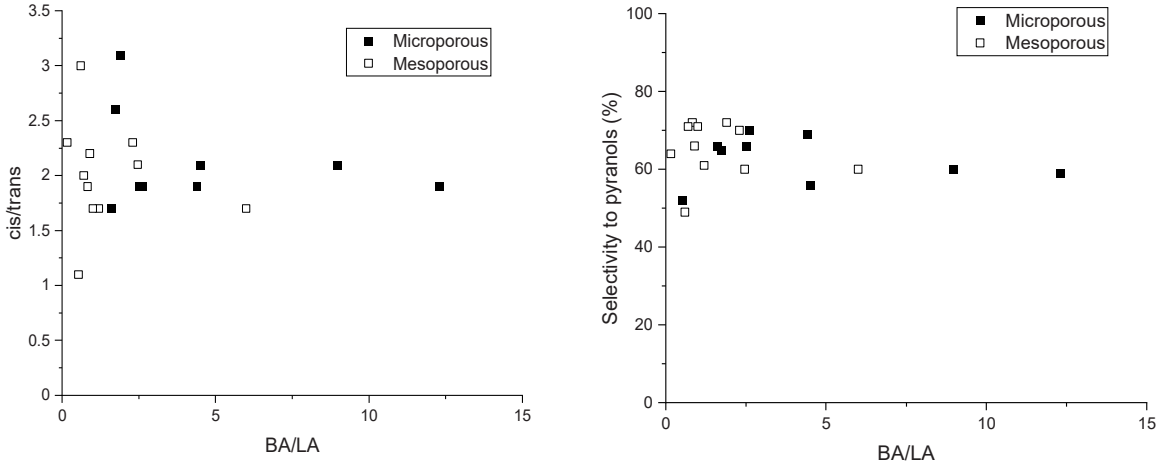

Fig. 10. Cis/trans ratio and selectivity to pyranols as a function of BA/LA ratio of the catalyst. Data is taken from the current work and references [21–23].

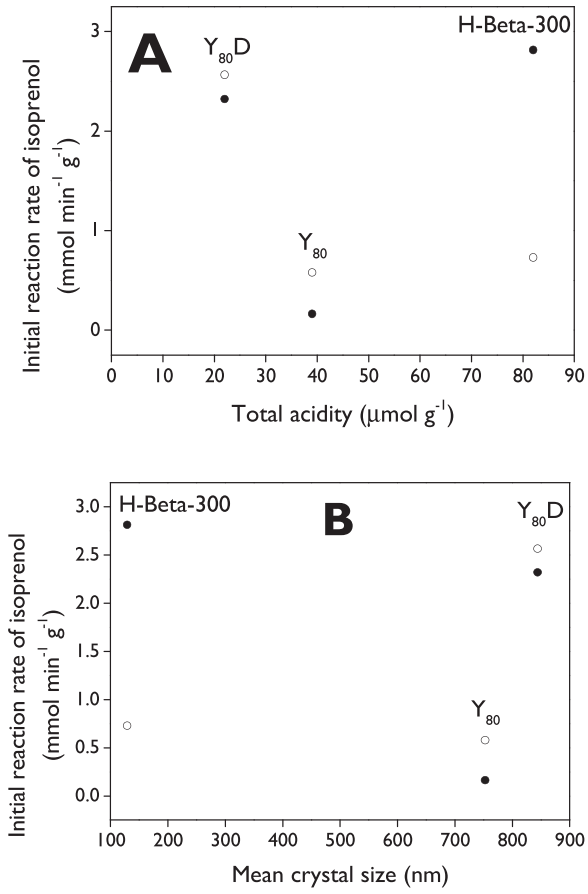

Fig. 11. Initial reaction rates for isoprenol as a function of (A) the total acidity of the catalyst and (B) crystal size of the catalyst at 40 °C (open symbol) and 60 °C (solid symbol). Data for H-Beta-300 taken from [22]. Reaction conditions: $C_{IP,0}$ = 0.2 mol L^{-1}, $C_{IVA,0}$ = 1.0 mol L^{-1}, 25 mL total volume, dimethyl carbonate as a solvent, 75 mg of catalyst, 1400 rpm.

levels were obtained with dealuminated catalysts, while microporous Sn_2Y_{80}EIM exhibited the lowest conversion (Fig. 8a). One reason for its low activity is the smallest surface area among all studied catalysts (Table 2).

Conversion of isoprenol at 120 min as a function of BA/LA ratio of different catalysts is shown in Fig. 9a. The highest final conversions were obtained with the catalysts exhibiting BA/LA ratio in the range of 1.2 – 12.3 over both microporous ($Sn_2Y_{5.1}$EIM, Y_{30}) and mesoporous catalysts (Sn_4Y_{30}D), while rather low conversion levels were obtained with $Y_{5.1}$ and Sn_4Y_{80}EIM. $Y_{5.1}$ exhibited also very high total acidity. The reason for the low activity for $Sn_4Y_{5.1}$EIM is its too high BA/LA ratio promoting deactivation. The low final conversion of Sn_2Y_{80}EIM is difficult to be explained because it has neither too high acid concentration nor too high amount of strong Brønsted acid sites.

3.2.3. *Product distribution*

Selectivity to pyranol was the highest over $Sn_2Y_{5.1}$EIM which exhibited a low amount of Lewis acid sites and a high amount of strong Brønsted acid sites (Table 3). Most probably not all these sites are available for the reaction, because both pyranol and dihydropyran have larger sizes in comparison to the pore size. All other $Y_{5.1}$ catalysts deactivated and gave low selectivity to both pyranol and dihydropyran (Figs. 6b, 6d, Table 5). The highest cis/trans pyranol ratio for H-Y-5.1 supported catalysts was obtained over mesoporous $Sn_4Y_{5.1}$D, although at a rather low conversion level (Fig. 6c).

Selectivity to pyranols increased with increasing conversion for H-Y-30 catalysts and the highest selectivity was obtained with tin modified microporous catalysts (Fig. 7b), while dealuminated catalysts exhibited lower selectivity. Cis pyranol formation was favored over microporous tin modified Sn_2Y_{30}EIM and Sn_4Y_{30}EIM catalysts, which also exhibited a lower BA/LA ratio, but a higher amount of strong Brønsted acid sites in comparison to the parent H-Y-30 (Fig. 7c, Table 3). Dealuminated Y_{30}D and Sn_4Y_{30}D gave on the other hand, a slightly lower cis/trans pyranol ratio, ca. 1.6 at high conversion levels (Fig. 7c) analogously to mesoporous H-MCM-41 [22]. Dihydropyran and pyranol are formed in a parallel manner as shown in Fig. 7e and confirmed also in Fig. 1, and the formation of dihydropyran was lower over microporous than with mesoporous catalysts. The ratios of the initial dihydropyran formation rate per initial pyranol formation rate are given in Table 5. Especially this ratio was high for Sn_4Y_{30}D which exhibited a rather low amount of strong acid sites (Table 3) indicating that mesoporosity is beneficial for dehydration reaction. When plotting the concentration of dihydropyranol as a function of pyranol concentration, it can be seen that more intensive dehydration occurred with dealuminated Y_{30}D and Sn_4Y_{30}D in comparison to microporous Y_{30} and tin modified Y_{30} catalysts (Fig. 7d). This is explained by the presence of large pores facilitating further reaction of pyranol, while for microporous catalysts the reaction occurred on the external surface or pore mouth of the catalyst.

For Y_{80} series catalysts, selectivity to pyranol was nearly independent on the catalyst (Fig. 8b). For H-Y-80 supported catalysts the cis/trans ratio decreased with increasing conversion and this ratio was nearly independent on the catalyst (Fig. 8c). The lowest cis/trans ratio was observed at 70% conversion for Sn_4Y_{80}EIM containing also a

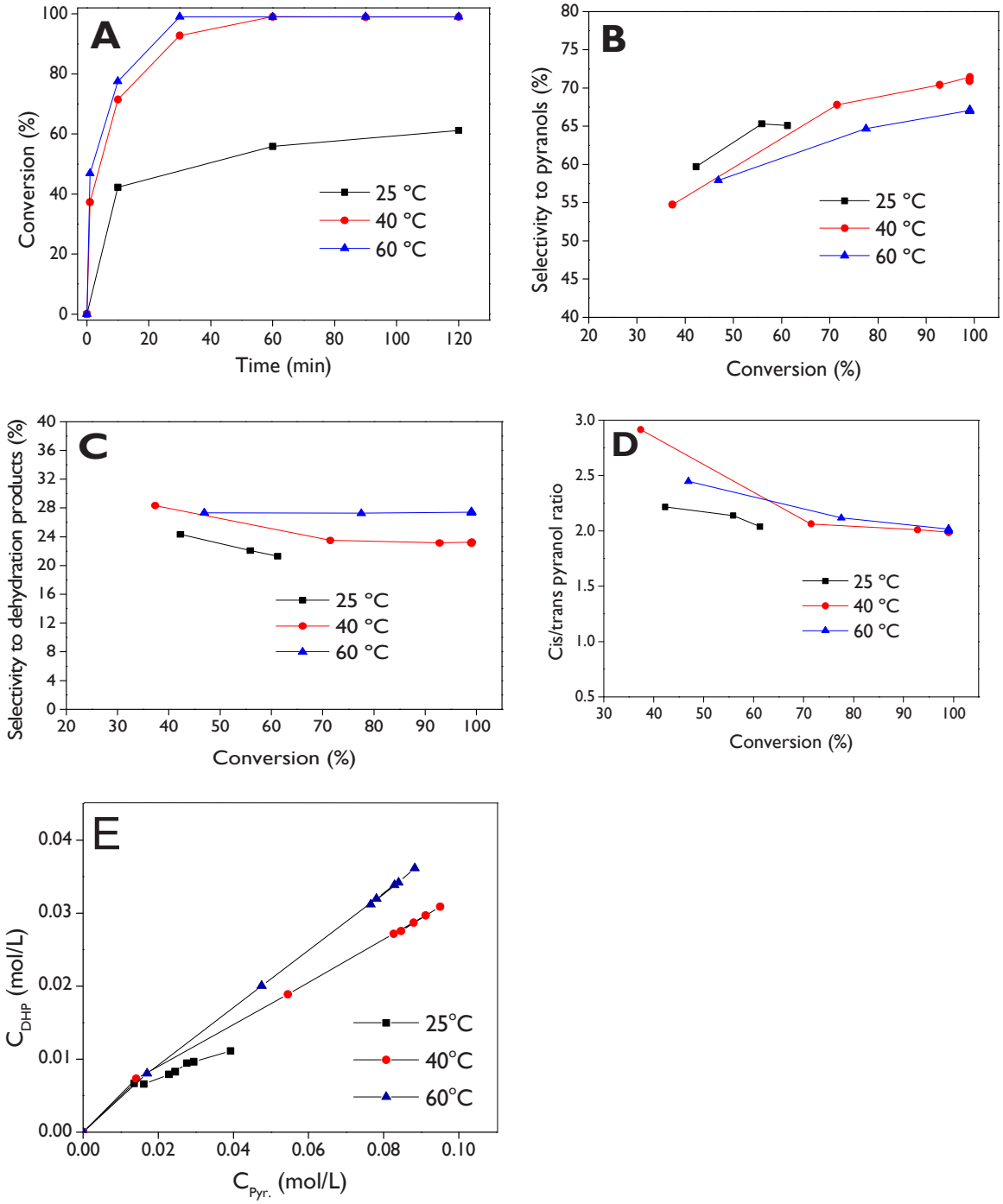

Fig. 12. Effect of the temperature on the Prins cyclization of isoprenol over $Y_{80}D$: (A) Dependence of the isoprenol conversion with the reaction time, (B) selectivity to pyranols, (C) selectivity to dehydration products, (D) cis/trans pyranol ratio as a function of conversion, and (E) concentration of dihydropyrans as vs concentration of pyranols. Reaction conditions: $C_{IP,0} = 0.2$ mol L^{-1}, $C_{IVA,0} = 1.0$ mol L^{-1}, 25 mL total volume, dimethyl carbonate as a solvent, 75 mg of catalyst, 1400 rpm.

relatively large amount of strong Brønsted acid sites (Table 3). The highest formation of dehydration products occurred over microporous Sn_4Y_{80}EIM exhibiting the BA/LA ratio of 2.6, which is the highest among this series (Fig. 8d, Table 3). For this catalyst, the initial DHP formation rate was very high, while after 10 min of the reaction, the $r_{0,DHP}/r_{0,Pyr}$ decreased from 1.1 to 0.08 due to deactivation of the acidic sites (Fig. 8d). Furthermore, Sn_4Y_{80}EIM contained high amounts of strong acid sites.

To rationalize the results, conversion and selectivity to pyranols were plotted as a function of BA/LA ratio (Figs. 9a, 9b). Furthermore, it was also worth to investigate the influence of mesoporosity on pyranol selectivity and the cis/trans ratio (Figs. 9c, 9d). The highest selectivity to pyranols at 70% conversion was obtained with Sn_4Y_{80}EIM exhibiting BA/LA ratio of 2.6 and containing both strong Brønsted and Lewis acid sites. The desired isomer of pyranol is cis and the highest cis/trans ratio was obtained over $Y_{80}D$ with a low BA/LA ratio and low total acidity.

Overall, the highest selectivity to pyranols was obtained at 70% conversion level for Sn_4Y_{80}EIM followed by Sn_2Y_{30}EIM, while in the absence of tin slightly lower selectivity was obtained for Y_{80} and $Y_{80}D$ (Table 5). The two best microporous catalysts exhibited BA/LA ratio in the range of 2.6–4.4 and a rather high amount of strong Brønsted acid sites as well as a high amount of Lewis acid sites. Slightly lower

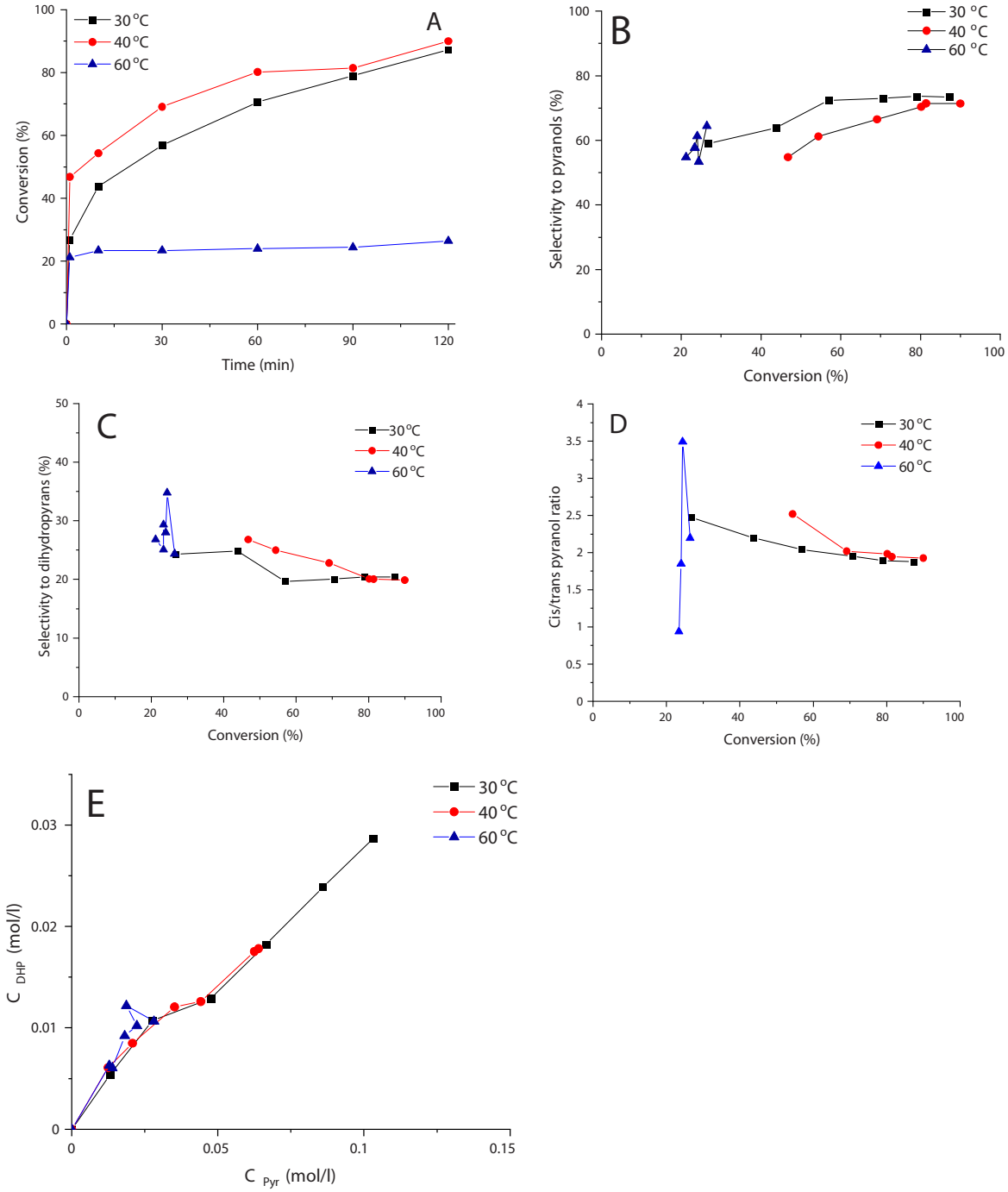

Fig. 13. Effect of the temperature on the Prins cyclization of isoprenol over Y_{80}: (A) Dependence of the isoprenol conversion with the reaction time, (B) selectivity to pyranols, (C) selectivity to dehydration products, (D) cis/trans pyranol ratio as a function of conversion, and (E) concentration of dihydropyrans vs concentration of pyranols. Reaction conditions:$C_{IP,0} = 0.2$ mol L^{-1}, $C_{IVA,0} = 1.0$ mol L^{-1}, 25 mL total volume, dimethyl carbonate as a solvent, 75 mg of catalyst, 1400 rpm.

selectivity to pyranols formed over Y_{80} and $Y_{80}D$ can be due to their much lower Lewis acid site concentration. In addition, it should be pointed out here that Y_{80} and $Y_{80}D$ catalysts were efficient in transformations of isoprenol to pyranols even though they exhibited a low amount of Brønsted acid sites and the latter one with mesoporous exhibited 7.8-fold higher initial TOF than the microporous one.

As a comparison, the highest selectivity to pyranols was reported with HPMo/MCM-41 in [18]. However, leaching of the heteropolyacid was observed. The high selectivity to pyranols of ca. 80% over $CsH_3PW_{12}O_{40}$ was obtained under optimized conditions with a 10-fold excess of isovaleraldehyde and in the presence of a small amount of water together with dimethyl carbonate, while in the absence of water only 76% selectivity to pyranols was obtained [19]. High selectivity (above 70%) was obtained for pyranols over acidic $FeCl_3/SiO_2$ and K-10, K-30 clays as well as hierarchical zeolites [21–23]. It is also difficult to correlate catalyst properties with their performance if acidity of the catalyst has not been determined [19]. On the other hand, rather low pyranol selectivity was obtained over MoO_3/SiO_2 [49]. For those studies with known catalyst acidities, a comparison has been made (Table S1, Fig. 10). The results show that cis/trans ratio of pyranols was the highest for both micro- and mesoporous catalysts with low BA/LA ratio, although low BA/LA ratio can result in low cis/trans ratio. The

Table 6
Initial reaction rates for isoprenol, conversion, and selectivity to pyranol at different temperatures.

Catalyst	Temperature	$r_{0,IP}$ (mol/s/g_{cat})	X (%) after 120 min	S (%)[a]
Y_{80}	30	0.03	87	74
Y_{80}	40	0.58	90	70
Y_{80}	60	0.16	25	n.a.
$Y_{80}D$	40	0.58	99	68
$Y_{80}D$	60	0.16	99	67
H-Beta-300	40	0.73	99	70
H-Beta-300	60	2.81	99	72

n.a. not available.
[a] 80% conversion,

Table 7
The ratio between the initial reaction rate for dihydropyran vs isoprenol, $r_{0,DHP}/r_{0,IP}$ and the same ratio after prolonged time $r_{t,DHP}/r_{t,IP}$ at different temperatures.

Catalyst	Temperature (°C)	$r_{0,DHP}/r_{0,IP}$	$r_{t,DHP}/r_{t,IP}$
Y_{80}	30	0.42	0.23
Y_{80}	40	0.42	0.23
Y_{80}	60	0.42	0.23
$Y_{80}D$	40	0.58	0.27
$Y_{80}D$	60	0.58	0.11
H-Beta-300 [22]	40	0.28	0.05[a]
H-Beta-300 [22]	60	0.33	0.36

[a] the slope after 30 min reaction time

selectivity to pyranols was also high with the catalyst exhibiting low BA/LA ratio. When plotting cis/trans ratio and selectivity to pyranols as a function of total acidity, no clear correlation was observed, thus the type of acid sites is more important than the total catalyst acidity.

3.2.4. *Effect of the temperature*

The effect of temperature was investigated over microporous Y_{80} and its mesoporous counterpart $Y_{80}D$ (Figs. 11–13, Table 6). The results showed that the initial rate for both catalysts unexpectedly decreased with increasing temperature from 40 °C to 60 °C, while a normal increase to the initial rate with increasing temperature was observed over H-Beta-300 [22]. The only difference in Y_{80}, $Y_{80}D$ and H-Beta-300 catalysts are their different BA/LA ratio and total acidity. The BA/LA ratio of Y_{80}, $Y_{80}D$ and H-Beta-300 were 1.6, 0.16, and 1.93, respectively and the corresponding total acidities were 39, 22, and 82 μmol g^{-1}, respectively. When plotting the initial rates for isoprenol reaction as a function of total acidity (Fig. 11a), it can be seen that H-Beta-300 with its higher total acidity was active even at 60 °C. One reason for the declined activity of microporous catalysts with low total acidity is that the product molecules block the pores, and thus there is not enough acidity on the external catalyst surface for Y_{80} and $Y_{80}D$ catalysts.

Another parameter, the average crystal size of different catalysts, has also an effect on the initial reaction rates for isoprenol as depicted in Fig. 11b. The results showed that for H-Beta-300 with a small average crystal size of 129 nm, the initial isoprenol reaction rate increased with increasing temperature as expected, while for the two other catalysts lower initial reaction rates were obtained at higher temperatures (Fig. 11b).

After prolonged time nearly complete conversion was obtained at 40 °C and 60 °C over $Y_{80}D$, while at 25 °C this catalyst exhibited low activity giving only 53% conversion in 2 h (Fig. 12a). Pyranol selectivity was inversely dependent on temperature (Fig. 12b), which is explained by the higher selectivity to dehydration products at higher temperature (Fig. 12c). On the other hand, the lowest cis/trans ratio of pyranol was obtained at 25 °C (Fig. 12d). Parallel formation of pyranol and dehydrated product was observed, however, dehydrated product concentration was increased with increasing temperature, as expected (Fig. 12e) [22].

For microporous Y_{80} catalyst the effect of temperature was unexpected (Fig. 13a). The catalyst was fully deactivated after 1 min reaction time at 60 °C, which is explained by its microporosity, large crystal size and relatively low total acidity, while the highest conversion was obtained at 40 °C. Rapid catalyst deactivation occurred also in the same reaction at 40 °C even for two hierarchical zeolites exhibiting the largest crystal sizes [23].

Low temperature, 30 °C was beneficial for the highest selectivity to pyranol (Fig. 13b) as was also reported in [19]. Selectivity to pyranols increased with increasing conversion when the opposite was observed for DHP selectivity (Figs. 13b, 13c).

The cis/trans pyranol ratio (Fig. 13d) decreased at 30 °C and 40 °C with increasing conversion analogously to Fig. 12d for $Y_{80}D$. Interestingly no difference of the parallel formation of dihydropyran and pyranol was observed in the temperature range of 30–60 °C (Fig. 13e). The corresponding picture for H-Beta-300 is depicted in Figure S8, which shows the highest dihydropyran formation at 60 °C [22]. When comparing the ratio between the initial formation rates of dihydropyran to pyranol $r_{0,DHP}/r_{0,IP}$ and the same ratio after prolonged time $r_{t,DHP}/r_{t,IP}$ (Table 7) for Y_{80}, $Y_{80}D$ and H-Beta-300 [22], it can be seen that $r_{0,DHP}/r_{0,IP}$ decreased in the following order: H-Beta-300> Y_{80} > $Y_{80}D$ while after prolonged time $r_{t,DHP}/r_{t,IP}$ was constant for Y_{80} at different temperatures, whereas for $Y_{80}D$ it was the lowest at 60 °C indicating more prominent deactivation of the acid sites. On the other hand, for H-Beta-300, $r_{0,DHP}/r_{0,IP}$ was nearly the same as $r_{t,DHP}/r_{t,IP}$ and this catalyst was very active at 60 °C due its smaller crystal size, a higher

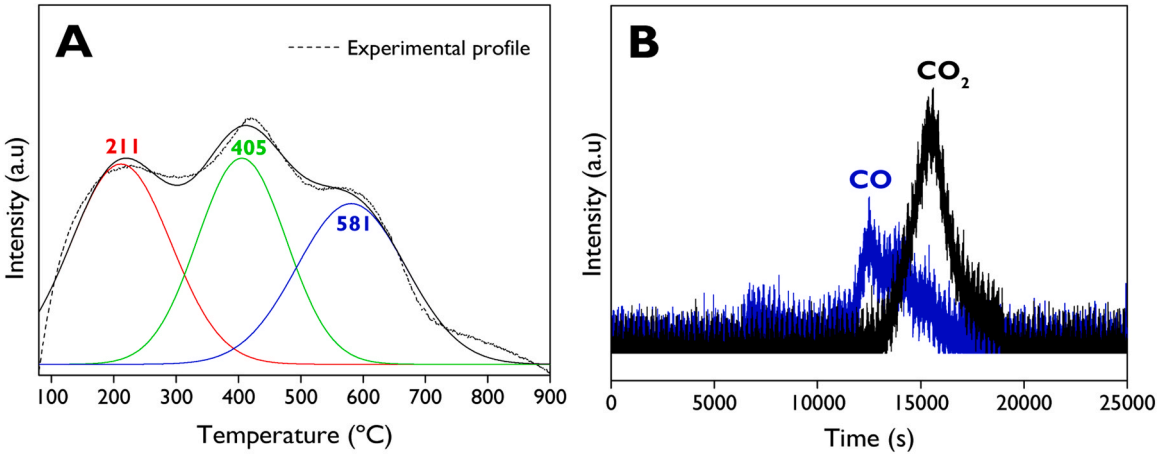

Fig. 14. (A) O_2-TPO profile and (B) In-situ mass spectrometry, for the spent $Y_{80}D$ catalyst.

BA/LA ratio in comparison to other two catalysts.

3.3. Catalyst robustness

The reuse of the $Y_{80}D$ catalyst was investigated after washing with acetone and calcination of the spent catalyst at 400 °C. These conditions are apparently not sufficient as it was not possible to convert all isoprenol with conversion remaining at ca. 78% level after 120 min, while for the fresh catalyst the conversion was 99% (Figure S9). Although selectivity to pyranol remained nearly the same as for the fresh catalyst, the cis/trans pyranol ratio was also 10% lower than for the fresh catalyst. TPO results (Fig. 14) of the spent catalyst showed the presence of a peak at 211 ºC, associated with soft coke, and peaks at 405 and 581 ºC associated with hard coke [50]. This result was also different from the one obtained with H-Beta-300 [22], which could be fully regenerated in reuse.

4. Conclusions

Prins cyclization of isoprenol with isovaleraldehyde was investigated over parent, dealuminated and Sn-modified Y-zeolites with different SiO_2/Al_2O_3 ratios. Tin was loaded with the evaporation impregnation method giving the particle size in the range of 2–11 nm.

The highest initial turnover frequency was obtained for dealuminated $Y_{80}D$ zeolite exhibiting low acidity and large pores, while for microporous zeolites the initial TOF values were very small. For tin modified catalysts, mesoporous, hierarchical $Sn_4Y_{80}D$ and $Sn_2Y_{30}D$ (Sn_4 =$SnCl_4$, Sn_2 = $SnCl_2$, D = dealuminated) exhibited higher initial turnover frequencies in comparison to their microporous counterparts. The hierarchical zeolites were active due to their large pore size in comparison to the product size.

The selectivity to the desired pyranols compared at 70% conversion level of isoprenol was the highest for tin modified microporous Sn_2Y_{30}EIM and Sn_4Y_{80}EIM, being 69% and 70%, respectively. These catalysts exhibited an adequate Brønsted to Lewis acid site ratio and high amount of Lewis acid sites, which promoted pyranol formation.

The effect of temperature was investigated over microporous Y_{80} catalyst in the temperature range of 30–60 °C. The results showed that this catalyst was very efficient at 30 °C and 40 °C, while at 60 °C a rapid catalyst deactivation occurred. This result was explained by a relatively large crystallite size of Y_{80} particles. Slightly higher selectivity to pyranols, 73%, was obtained at 30 °C in comparison to 40 °C.

CRediT authorship contribution statement

Mika Lastusaari: Investigation. **Kari Eränen:** Resources, Methodology. **Ilari Angervo:** Investigation. **Pascal Demuth:** Investigation. **Luis A. Gallego-Villada:** Writing – original draft, Investigation. **Dmitry Yu. Murzin:** Writing – review & editing, Project administration, Methodology, Conceptualization. **Zuzana Vajglová:** Investigation. **Narendra Kumar:** Supervision, Methodology. **Päivi Mäki-Arvela:** Writing – original draft, Supervision, Methodology, Conceptualization. **Ramin Majidov:** Investigation.

Declaration of Competing Interest

The authors declare that they have no known competing financial interests or personal relationships that could have appeared to influence the work reported in this paper.

Data availability

Data will be made available on request.

Acknowledgements

Luis A. Gallego-Villada is grateful to Universidad de Antioquia for their support during his research internship at Åbo Akademi University through the project 2022-53000 as a part of the "Convocatoria Programática 2021–2022: Ingeniería y Tecnología" program, as well as the "Beca Doctoral Universidad de Antioquia" scholarship.

Appendix A. Supporting information

Supplementary data associated with this article can be found in the online version at doi:10.1016/j.cattod.2024.114695.

References

[1] F. Doro, N. Akeroyd, F. Schiet, A. Narula, The Prins reaction in the fragrance industry: 100th anniversary (1919–2019), Angew. Chem. Int. Ed. 58 (2019) 7174–7179, https://doi.org/10.1002/anie.201814470.
[2] K.R.K.K. Reddy, L.F. Silva Junior, Iodine-catalyzed prins cyclization of aliphatic and aromatic ketones, J. Braz. Chem. Soc. 24 (2013) 1414–1419, https://doi.org/10.5935/0103-5053.20130178.
[3] Transparency Market Research, Isoprenol Market, Global Industry Report, 2030, (2020). ⟨https://www.transparencymarketresearch.com/isoprenol-market.html⟩ (Accessed 20 August 2023).
[4] W.F. Hoelderich, Environmentally benign manufacturing of fine and intermediate chemicals, Catal. Today 62 (2000) 115–130, https://doi.org/10.1016/S0920-5861(00)00413-2.
[5] W. Aquila, H. Fuchs, O. Wörz, W. Ruppel, K. Halbritteer, Continuous Industrial Production of Unsaturated Aliphatic Aldehydes in a Tube Bundle Reactor, 6,013,843, 2000.
[6] W. Bonrath, T. Netscher, Catalytic processes in vitamins synthesis and production, Appl. Catal. A Gen. 280 (2005) 55–73, https://doi.org/10.1016/j.apcata.2004.08.028.
[7] M. Dehn, B. Brunner, K. Ebel, S. Huber, Process for Producing Prenol and Prenal from Isoprenol, US 2019/0077736 A1, 2019.
[8] G. Wegner, G. Kaibel, J. Therre, A. Werner, H. Fuchs, Continuous Method for Producing Citral, WO 2008/037693 A1, 2008.
[9] M. Dyga, A. Keller, H. Hasse, Vapor–liquid equilibria and chemical equilibria in the system (formaldehyde + water + isoprenol), Ind. Eng. Chem. Res. 60 (2021) 4471–4483, https://doi.org/10.1021/acs.iecr.1c00168.
[10] K. Kumar, J. Malhotra, S. Kumar, V. Sood, D. Singh, M. Sharma, R. Joshi, Citral enrichment in lemongrass (Cymbopogon flexuosus) oil using spinning band equipped high vacuum distillation column and sensory evaluation of fractions, Food Chem. Adv. 2 (2023) 100291, https://doi.org/10.1016/j.focha.2023.100291.
[11] A. Werner, M.B. Roig, A.-N. Parvulescu, R. Minges, A. Keller, S. Maurer, U. Mueller, W. Siegel, Process for Recovering 3-methylbut-3-en-1-ol, US 2020/0239394 A1, 2020.
[12] S. Wang, W. Zhao, T.S. Lee, S.W. Singer, B.A. Simmons, S. Singh, Q. Yuan, G. Cheng, Dimethyl sulfoxide assisted ionic liquid pretreatment of switchgrass for isoprenol production, ACS Sustain. Chem. Eng. 6 (2018) 4354–4361, https://doi.org/10.1021/acssuschemeng.7b04908.
[13] H. Liu, Y. Wang, Q. Tang, W. Kong, W.-J. Chung, T. Lu, MEP pathway-mediated isopentenol production in metabolically engineered Escherichia coli, Microb. Cell Fact. 13 (2014) 135, https://doi.org/10.1186/s12934-014-0135-y.
[14] A. Kang, D. Mendez-Perez, E.-B. Goh, E.E.K. Baidoo, V.T. Benites, H.R. Beller, J. D. Keasling, P.D. Adams, A. Mukhopadhyay, T.S. Lee, Optimization of the IPP-bypass mevalonate pathway and fed-batch fermentation for the production of isoprenol in Escherichia coli, Metab. Eng. 56 (2019) 85–96, https://doi.org/10.1016/j.ymben.2019.09.003.
[15] Transparency Market Research, Florol Market - Global Industry Analysis, Size, Share, Growth, Trends, and Forecast 2016-2024, (n.d.). ⟨https://www.transparencymarketresearch.com/florol-market.html⟩ (Accessed 22 August 2023).
[16] E. Vyskočilová, L. Rezková, E. Vrbková, I. Paterová, L. Červený, Contribution to elucidation of the mechanism of preparation of 2-isobutyl-4-methyltetrahydro-2H-pyran-4-ol, Res. Chem. Intermed. 42 (2016) 725–733, https://doi.org/10.1007/s11164-015-2052-z.
[17] G.P. More, M. Rane, S.V. Bhat, Efficient Prins cyclization in environmentally benign method using ion exchange resin catalyst, Green Chem. Lett. Rev. 5 (2012) 13–17, https://doi.org/10.1080/17518253.2011.572929.
[18] E. Vyskočilová, M. Krátká, M. Veselý, E. Vrbková, L. Červený, Prins cyclization for the preparation of 2-isobutyl-4-methyl-tetrahydro-2H-pyran-4-ol using supported heteropoly acids, Res. Chem. Intermed. 42 (2016) 6991–7003, https://doi.org/10.1007/s11164-016-2511-1.
[19] A.L.P. de Meireles, K.A. da Silva Rocha, E.F. Kozhevnikova, I.V. Kozhevnikov, E. V. Gusevskaya, Heteropoly acid catalysts in Prins cyclization for the synthesis of Florol®, Mol. Catal. 502 (2021) 111382 https://doi.org/10.1016/j.mcat.2020.111382.
[20] L. Sekerová, E. Vyskočilová, J.S. Fantova, I. Paterová, J. Krupka, L. Červený, Preparation of 2-isobutyl-4-methyltetrahydro-2H-pyran-4-ol via Prins cyclization using Fe-modified silica, Res. Chem. Intermed. 43 (2017) 4943–4958, https://doi.org/10.1007/s11164-017-2922-7.

[21] A.Y. Sidorenko, Y.M. Kurban, A. Aho, Z.V. Ihnatovich, T.F. Kuznetsova, I. Heinmaa, D.Y. Murzin, V.E. Agabekov, Solvent-free synthesis of tetrahydropyran alcohols over acid-modified clays, Mol. Catal. 499 (2021) 111306, https://doi.org/10.1016/j.mcat.2020.111306.
[22] B. Lasne, P. Mäki-Arvela, A. Aho, Z. Vajglova, K. Eränen, N. Kumar, J.E. Sánchez-Velandia, M. Peurla, C. Mondelli, J. Pérez-Ramírez, D.Y. Murzin, Synthesis of Florol via Prins cyclization over heterogeneous catalysts, J. Catal. 405 (2022) 288–302, https://doi.org/10.1016/j.jcat.2021.12.008.
[23] N. Shcherban, R. Barakov, B. Lasne, P. Mäki-Arvela, M. Shamzhy, I. Bezverkhyy, J. Wärnå, D.Y. Murzin, Florol synthesis via Prins cyclization over hierarchical beta zeolites, Mol. Catal. 531 (2022) 112683, https://doi.org/10.1016/j.mcat.2022.112683.
[24] R. Barakov, N. Shcherban, P. Yaremov, I. Bezverkhyy, J. Čejka, M. Opanasenko, Hierarchical Beta zeolites as catalysts in a one-pot three-component cascade Prins–Friedel–Crafts reaction, Green. Chem. 22 (2020) 6992–7002, https://doi.org/10.1039/D0GC01787F.
[25] S.L. Suib, J. Přech, E. Szaniawska, J. Čejka, Recent advances in tetra- (Ti, Sn, Zr, Hf) and pentavalent (Nb, V, Ta) metal-substituted molecular sieve catalysis, Chem. Rev. 123 (2023) 877–917, https://doi.org/10.1021/acs.chemrev.2c00509.
[26] M. Opanasenko, A. Dhakshinamoorthy, Y.K. Hwang, J. Chang, H. Garcia, J. Čejka, Superior performance of metal–organic frameworks over zeolites as solid acid catalysts in the prins reaction: green synthesis of Nopol, ChemSusChem 6 (2013) 865–871, https://doi.org/10.1002/cssc.201300032.
[27] L.A. Gallego-Villada, E.A. Alarcón, A.L. Villa, Evaluation of nopol production obtained from turpentine oil over Sn/MCM-41 synthesized by wetness impregnation using the Central Composite Design, Mol. Catal. 498 (2020) 111250, https://doi.org/10.1016/j.mcat.2020.111250.
[28] L.A. Gallego-Villada, E.A. Alarcón, A.L. Villa, Effect of Colombian raw materials on the Prins condensation reaction over Sn/MCM-41, Catal. Today 372 (2021) 36–50, https://doi.org/10.1016/j.cattod.2020.10.040.
[29] Z. Yongzhong, N. Yuntong, S. Jaenicke, G. Chuah, Cyclisation of citronellal over zirconium zeolite beta? a highly diastereoselective catalyst to (.)-isopulegol, J. Catal. 229 (2005) 404–413, https://doi.org/10.1016/j.jcat.2004.11.015.
[30] A. Corma, M. Renz, Water-resistant Lewis-acid sites: carbonyl-ene reactions catalyzed by tin-containing, hydrophobic molecular sieves, Arkivoc 2007 (2007) 40–48, https://doi.org/10.3998/ark.5550190.0008.805.
[31] V.S. Marakatti, A.B. Halgeri, G.V. Shanbhag, Metal ion-exchanged zeolites as solid acid catalysts for the green synthesis of nopol from Prins reaction, Catal. Sci. Technol. 4 (2014) 4065–4074, https://doi.org/10.1039/C4CY00596A.
[32] J.M. Jimenez-Martin, A. Orozco-Saumell, H. Hernando, M. Linares, R. Mariscal, M. López Granados, A. García, J. Iglesias, Efficient conversion of glucose to methyl lactate with Sn-USY: retro-aldol activity promotion by controlled ion exchange, ACS Sustain. Chem. Eng. 10 (2022) 8885–8896, https://doi.org/10.1021/acssuschemeng.2c01987.
[33] R. Majidov, Sustainable Feedstock to Acrylic Acid using H-Y Zeolites (Master's thesis), Åbo Akademi, 2023. ⟨www.doria.fi/handle/10024/187633⟩.
[34] S. Engblom, A Study of Glucose Transformation to Lactic acid and Methyl lactate, Åbo Akademi University, 2020. ⟨https://www.doria.fi/handle/10024/180424⟩.
[35] C.A. Emeis, Determination of integrated molar extinction coefficients for infrared absorption bands of pyridine adsorbed on solid acid catalysts, J. Catal. 141 (1993) 347–354, https://doi.org/10.1006/jcat.1993.1145.
[36] J. Jeanjean, L. Aouali, D. Delafosse, A. Dereigne, Crystal structure of different dealuminated Y-type zeolites determination of framework vacancies and non-framework species, J. Chem. Soc. Faraday Trans. 1 Phys. Chem. Condens. Phases. 85 (1989) 2771–2783, https://doi.org/10.1039/f19898502771.
[37] W.H. Baur, A.A. Khan, Rutile-type compounds. IV. SiO2, GeO2 and a comparison with other rutile-type structures, Acta Crystallogr. Sect. B Struct. Crystallogr. Cryst. Chem. 27 (1971) 2133–2139, https://doi.org/10.1107/S0567740871005466.
[38] K.P. de Jong, J. Zečević, H. Friedrich, P.E. de Jongh, M. Bulut, S. van Donk, R. Kenmogne, A. Finiels, V. Hulea, F. Fajula, Zeolite Y Crystals with trimodal porosity as ideal hydrocracking catalysts, Angew. Chem. Int. Ed. 49 (2010) 10074–10078, https://doi.org/10.1002/anie.201004360.
[39] K. Sato, Y. Nishimura, H. Shimada, Preparation and activity evaluation of Y zeolites with or without mesoporosity, Catal. Lett. 60 (1999) 83–87, https://doi.org/10.1023/a:1019013830885.
[40] O. Vassylyev, J. Chen, G.S. Hall, J.G. Khinast, Efficient surface functionalization of zeolites via esterification, Microporous Mesoporous Mater. 92 (2006) 101–108, https://doi.org/10.1016/j.micromeso.2005.10.030.
[41] W.H. Baur, R.X. Fischer, The floppiness of it all: bond lengths change with atomic displacement parameters and the flexibility of various coordination tetrahedra in zeolitic frameworks. an empirical structural study of bond lengths and angles, Chem. Mater. 31 (2019) 2401–2420, https://doi.org/10.1021/acs.chemmater.8b04919.
[42] P.Y. Dapsens, C. Mondelli, J. Pérez-Ramírez, Design of Lewis-acid centres in zeolitic matrices for the conversion of renewables, Chem. Soc. Rev. 44 (2015) 7025–7043, https://doi.org/10.1039/C5CS00028A.
[43] K.S.W. Sing, Reporting physisorption data for gas/solid systems with special reference to the determination of surface area and porosity (Recommendations 1984), Pure Appl. Chem. 57 (1985) 603–619, https://doi.org/10.1351/pac198557040603.
[44] V. Palomba, A. Frazzica, Modeling of sorption systems for thermal energy storage. Adv. Therm. Energy Storage Syst., Elsevier, 2021, pp. 453–475, https://doi.org/10.1016/B978-0-12-819885-8.00015-2.
[45] S. Shimizu, N. Matubayasi, Surface area estimation: replacing the Brunauer–Emmett–Teller model with the statistical thermodynamic fluctuation theory, Langmuir 38 (2022) 7989–8002, https://doi.org/10.1021/acs.langmuir.2c00753.
[46] K.S. Triantafyllidis, S.A. Karakoulia, D. Gournis, A. Delimitis, L. Nalbandian, E. Maccallini, P. Rudolf, Formation of carbon nanotubes on iron/cobalt oxides supported on zeolite-Y: Effect of zeolite textural properties and particle morphology, Microporous Mesoporous Mater. 110 (2008) 128–140, https://doi.org/10.1016/j.micromeso.2007.10.007.
[47] Z. Vajglová, N. Kumar, P. Mäki-Arvela, K. Eränen, M. Peurla, L. Hupa, M. Nurmi, M. Toivakka, D.Y. Murzin, Synthesis and Physicochemical characterization of shaped catalysts of β and y zeolites for cyclization of citronellal, Ind. Eng. Chem. Res. 58 (2019) 18084–18096, https://doi.org/10.1021/acs.iecr.9b02829.
[48] A.Y. Sidorenko, Y.M. Kurban, A.V. Kravtsova, I.V. Il'ina, N.S. Li-Zhulanov, D. V. Korchagina, J.E. Sánchez-Velandia, A. Aho, K.P. Volcho, N.F. Salakhutdinov, D. Y. Murzin, V.E. Agabekov, Clays catalyzed cascade Prins and Prins-Friedel-Crafts reactions for synthesis of terpenoid-derived polycyclic compounds, Appl. Catal. A Gen. 629 (2022) 118395, https://doi.org/10.1016/j.apcata.2021.118395.
[49] L. Sekerová, E. Vyskočilová, L. Červený, Prins cyclization of isoprenol with various aldehydes using MoO3/SiO2 as a catalyst, React. Kinet. Mech. Catal. 121 (2017) 83–95, https://doi.org/10.1007/s11144-016-1131-5.
[50] M. Díaz, E. Epelde, J. Valecillos, S. Izaddoust, A.T. Aguayo, J. Bilbao, Coke deactivation and regeneration of HZSM-5 zeolite catalysts in the oligomerization of 1-butene, Appl. Catal. B Environ. 291 (2021) 120076, https://doi.org/10.1016/j.apcatb.2021.120076.